Local scale depositional processes of surface snow on the Greenland ice sheet

Alexandra M. Zuhr[1,2], Thomas Münch[1], Hans Christian Steen-Larsen[3], Maria Hörhold[4], and Thomas Laepple[1,5]

[1]Alfred-Wegener-Institut Helmholtz Zentrum für Polar- und Meeresforschung, Research Unit Potsdam, Telegrafenberg A45, 14473 Potsdam, Germany
[2]University of Potsdam, Institute of Geosciences, Karl-Liebknecht-Str. 24-25, 14476 Potsdam-Golm, Germany
[3]Geophysical Institute, University of Bergen and Bjerknes Centre for Climate Research, Bergen, Norway
[4]Alfred-Wegener-Institut Helmholtz Zentrum für Polar- und Meeresforschung, Research Unit Bremerhaven, 27568 Bremerhaven, Germany
[5]University of Bremen, MARUM - Center for Marine Environmental Sciences and Faculty of Geosciences, 28334 Bremen, Germany

Correspondence: Alexandra Zuhr (alexandra.zuhr@awi.de)

Abstract.

Ice cores from polar ice sheets and glaciers are an important climate archive. Snow layers, consecutively deposited and buried, contain climatic information of the time of their formation. However, particularly low-accumulation areas are characterised by temporally intermittent precipitation, which can be further re-distributed after initial deposition. Therefore, the local conditions

5 of accumulation at an ice core site influence the quantity and quality of the recorded climate signal in proxy records. Local surface features at different spatial scales further affect the signal imprint. This study therefore aims to characterise the local accumulation patterns and the evolution of the snow height to describe the contribution of snow (re-)deposition to noise in climate records from ice cores. By using a photogrammetry Structure-from-Motion approach, we generated near-daily elevation models of the snow surface for a 195 m² area in the vicinity of the deep drilling site of the East Greenland Ice Core Project in

10 northeast Greenland. Based on the snow height information we derived snow height changes on a day-to-day basis throughout our observation period from May to August 2018. Specifically, the average snow height increased by ∼11 cm. The spatial and temporal data set allowed an investigation of snow deposition versus depositional modifications. We observed irregular snow deposition, erosion, and the re-distribution of snow, which caused uneven snow accumulation patterns, a removal of more than 60 % of the deposited snow, and a negative relationship between the initial snow height and the amount of accumulated

15 snow. Furthermore, the surface roughness decreased from 4 to 2 cm throughout the spring and summer season at our study site. Finally, our study further shows that our method has several advantages over previous approaches, making it possible to demonstrate the importance of accumulation intermittency, and the potential influences of depositional processes on proxy signals in snow and ice.

1 Introduction

20 Ice cores from polar ice sheets and glaciers are one of the most important climate archives. Physical and chemical characteristics preserved in the ice store information on past climatic conditions and are used as proxy data, for example to reconstruct past temperatures (e.g., Dansgaard, 1964; Jouzel and Merlivat, 1984) or accumulation rates (e.g., Mosley-Thompson et al., 2001; Dethloff et al., 2002).

The accuracy and interpretability of reconstructed parameters depend on the understanding of the signal formation and the

25 processes that potentially change the original signal which is imprinted in the deposited precipitation. Amongst these are local processes such as snow-air exchange, alteration of the isotopic composition (Steen-Larsen et al., 2014; Ritter et al., 2016), depositional losses of chemical compounds (Weller et al., 2004), local to regional processes such as the spatial variability in snowfall leading to stratigraphic noise (Münch et al., 2017), and larger processes such as precipitation intermittency (Persson et al., 2011).

30 One major obstacle is the apparent gap between precipitation - as determined from model approaches, re-analysis data, and remote sensing products - and the net snow accumulation deposited at one specific location. This gap is caused by processes such as snow erosion, drift, and re-distribution which depend on the wind speed, wind direction, and duration of wind events, as well as the conditions of the snow surface (Li and Pomeroy, 1997a,b; Sturm et al., 2001). Surface features such as ripples and dunes are one result of spatially variable accumulation which alters the location and the amount of snow deposition. Loose

35 snow on top of consolidated features can easily be picked up, transported by wind, and re-deposited (Fisher et al., 1985; Albert and Hawley, 2002; Naaim-Bouvet et al., 2016). Depositional modifications of the snowpack further influence recorded climatic parameters in the snow. This study will therefore focus on characterising the temporal and spatial variability of snow accumulation.

The mapping of snowfall events, snow surface changes, and surface roughness is important to understand the temporal

40 variability of snow accumulation. The quantification of these parameters can help ascertain their contribution to precipitation intermittency and spatial variability as well as their impacts on the observed variability in a proxy record (van der Veen and Bolzan, 1999). The acquisition of reliable snow height data is still a challenge (Eisen et al., 2008). Methods to measure the amount of snow accumulation include stake lines and farms, snow height sensors, remote sensing products, photogrammetry and Structure-from-Motion (SfM), as well as laser scanning approaches. Stake lines, grids, and farms are a robust and low-cost

45 way to manually document snow height evolution (e.g., Kuhns et al., 1997; Mosley-Thompson et al., 1999; Schlosser et al., 2002); however, these methods require time and personnel in the field. A newer technique that requires less manual work is the use of sonic height sensors, which are often mounted next to an automatic weather station (AWS) (e.g., Steffen and Box, 2001; van de Wal et al., 2005). These sensors can provide measurements at a very high temporal resolution, but are restricted to a single point. Remote sensing products provide large spatial coverage; however, their large spatial resolution is not suitable for

50 small or local scale studies and estimates (e.g., van der Veen and Bolzan, 1999; Rignot and Thomas, 2002; Arthern et al., 2006). To obtain snow height changes on the scale from centimetres to kilometres, various forms of photogrammetry (Keutterling and Thomas, 2006; Basnet et al., 2016; Cimoli et al., 2017), SfM (Westoby et al., 2012; Fonstad et al., 2013; Nolan et al., 2015;

Smith et al., 2016), laser scanners (Baltsavias et al., 2001; Picard et al., 2016, 2019), and large grids of individual points (Mosley-Thompson et al., 1999; Schlosser et al., 2002) are used.

55 A variety of measurement techniques for snow accumulation is available, but most of these techniques are limited either in space, time, or feasibility. In this study, we introduce and use a photogrammetry Structure-from-Motion (SfM) approach to obtain snow height information as well as to investigate spatial and temporal snow accumulation and depositional modifications of the snow surface in the vicinity of the deep drilling site of the East Greenland Ice-Core Project (EGRIP) in northeast Greenland. By analysing the spatial and temporal variability of snowfall, we observe that less than half of the precipitated

60 and drifted snow is actually deposited. We further identify the processes of snow erosion, drift, and re-distribution as relevant factors being responsible for the change in surface roughness and the levelling out of surface features.

2 Data and Methods

2.1 Study Site

Our study site is located next to the EGRIP camp site in northeast Greenland (75° 38' N, 36° W, 2708 m a.s.l., Fig. 1a) (Dahl-
65 Jensen et al., 2019) with a mean annual temperature of -29 °C. The location is characterised by prevailing westerly winds (Madsen et al., 2019) with a mean wind direction of 252° during our observation period (Fig. A1). Accumulation rates in the vicinity of EGRIP are 13.9 cm w.eq. yr^{-1} as estimated over a period of ∼5 years from 2011 to 2015 (Schaller et al., 2016), while shallow ice cores and geophysical surveys indicate annual layer thicknesses between 11 and 13 cm of ice (Vallelonga et al., 2014; Karlsson et al., 2020). An AWS from the Program for the Monitoring of the Greenland Ice Sheet (PROMICE) (Ahlstrøm
70 et al., 2008) was installed in 2016 ∼ 500 m southeast of the camp (Fig. 1b) and provides meteorological data with a 10-minute resolution (Fig. A1). Since a variety of data from firn cores, snow pits, and snow-air exchange experiments are available for this site, it is an ideal location to study snow depositional processes and climate proxy formation.

2.2 Data and Structure from Motion Setup

In this study, we apply a photogrammetry SfM approach to map the daily snow accumulation patterns. To achieve this goal, we
75 took images of the snow surface covering a 39 x 10 m area, with the long x-axis set up perpendicular to the main wind direction and the short y-axis pointing towards it (referred as *Photogrammetry Area*; Fig. 1b). We set up 35 glass fiber sticks around the area (Fig. 1c) to provide absolute reference points for the snow surface height. All sticks were levelled to the same relative height by using a theodolite.

Photos were taken almost daily from 16th of May to 1st of August, 2018 (77 days), mostly between 6 and 8 pm (local camp
80 time, GMT-3) to ensure the best light contrast and similar light conditions on all photos (Nolan et al., 2015; Cimoli et al., 2017). No photos were taken on days with very cloudy or whiteout conditions. The photos were taken using a Sony α 6000 camera with a fixed lens of 20 mm focal length and a focal ratio of f/16. The ISO value was set to 100. These parameters were chosen to get as much contrast in the images as possible. The camera was mounted at a height of ∼ 1.6 m on a setup consisting
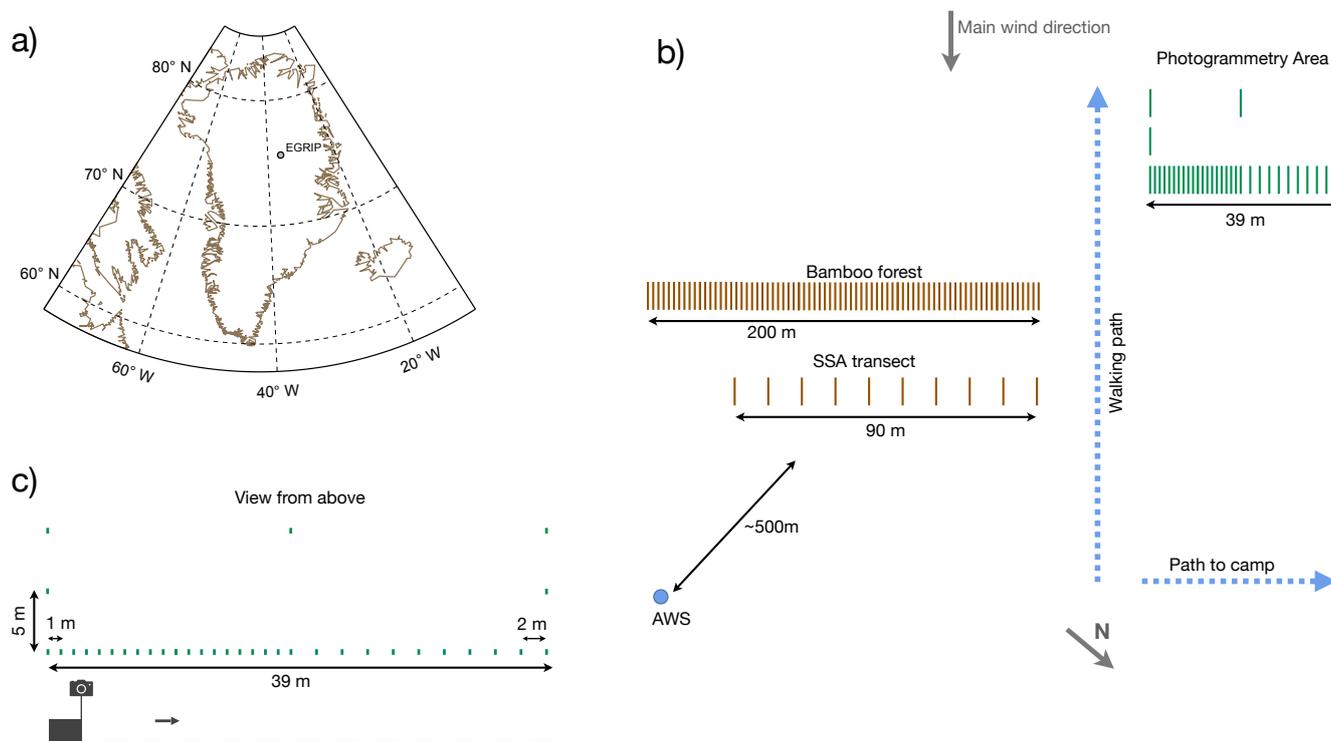
Figure 1. Overview maps for all relevant locations and transects. a) Map of Greenland with the location of the EGRIP camp site in northeast Greenland. b) Schematic map of the surface science area including all relevant study sites. This area is approximately 500 m south of the deep drilling site in the EGRIP camp. The map is not to scale. Data from the AWS, the Bamboo forest, and the SSA transect (SSA = Specific Surface Area) are used for the comparison of snow height estimates. c) Schematic illustration of the photogrammetry area with respective distances. 30 glass fiber sticks were set along the walking line, four sticks were positioned on the edges towards the main wind direction, and one in the back of the study area.

of a sledge, an ice core box, a plexiglass plate, and a metal pole (Fig. 2). During image acquisition, photos were taken every

85 second using an automatic shutter control while the sledge was dragged on foot by a person along the downwind main side (x-axis). This provided consecutive images with an overlap of ∼70 %. Due to overcast conditions affecting the light contrast, the inability to detect surface structures, failures in the image processing, or insufficient overlap of consecutive photos, we obtained an effective data set of 37 out of 77 days (48 %, Table A1).

  We used the software AgiSoft PhotoScan Professional (Version 1.4.3 Software, 2018, retrieved from http://www.agisoft.com/

90 downloads/installer/) for the SfM workflow including the digital elevation model (DEM) generation. DEMs have a resolution of 1 x 1 cm. For reliable geo-referencing, we manually added ground control points (GCPs) with known coordinates using the top of the glass fiber sticks (Fig. 1c) within Agisoft PhotoScan. The sticks at y=10 m are, however, not visible in every daily data set and cannot always be used as GCPs. Therefore, all 35 sticks are used as GCPs if they are visible, otherwise the effective
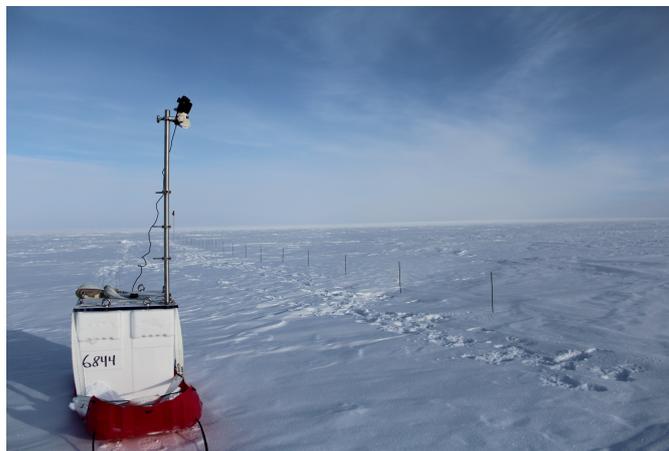
Figure 2. Camera setup for the image acquisition. The setup consists of a sledge, an ice core box, a plexiglass plate, a metal pole, and the camera used to take images of the study area.

number of GCPs varies between 32 and 35. The absence of the GCPs at y=10 m might impair the height control in the back of
95 the area. For further analyses, the study area was therefore restricted to y=5 m to ensure constant data availability.

Complementing the snow height data derived from our photogrammetry SfM approach (hereafter referred to as DEM (digital elevation model) and archived under https://doi.org/10.1594/PANGAEA.923418, Zuhr et al., 2020), four additional snow height evolution estimates are available with different temporal resolutions and spatial coverages (Table 1 and Fig. 1b): i) manual documentation of the relative snow height at the glass fiber sticks in the photogrammetry area (*PT sticks*, submitted to the
100 Pangaea database, DOI pending), ii) a 200 m long transect with 200 wooden sticks with 1 m spacing (*Bamboo forest*, archived under https://doi.pangaea.de/10.1594/PANGAEA.921855, Steen-Larsen, 2020a), iii) a 90 m long transect with 10 sticks and 10 m spacing (*SSA sticks*, SSA = specific surface area, archived under https://doi.pangaea.de/10.1594/PANGAEA.921853, Steen-Larsen, 2020b), and iv) a sonic snow height sensor at the nearby AWS (*AWS PROMICE*, http://www.promice.dk). The SSA stick line as well as the Bamboo forest were aligned in the same orientation as our study area. The high-resolution data
105 from the AWS PROMICE were summarised to daily values.

In addition to the photogrammetry SfM study, a snow sampling study was carried out downwind at the positions of the glass fibre sticks along the 39 m main line. After the sampling, the positions were filled up with snow to avoid drift and artificial surface structures. Even though we always flattened the sampling locations, we manually removed these areas in the DEM generation to minimise biased snow height estimates.

110 Snowfall was manually documented when snowfall samples were collected (Table A1). Both, snowfall and snowdrift lead to an increase in the snow height and a differentiation between these can be difficult in the DEMs. We therefore use our simple, manual documentation of snowfall (Table A1) as well as the ERA5 snowfall product from the European Centre for Medium-Range Weather Forecasts (ECMWF, 2017) to inform about the time of snowfall. ERA5 data were downloaded with an hourly resolution from the Climate Data Store (https://cds.climate.copernicus.eu) and summed up to daily values. If the

Table 1. Snow height estimates around the EGRIP camp site. The temporal resolution, the spatial extent, and the distance relative to the photogrammetry area are given. Bamboo forest and SSA stick estimates are averages across 200 or ten sticks, respectively. The single point high-resolution data from the AWS PROMICE were summarised to daily values. Locations are illustrated in the overview map (Fig. 1b).

Name	Temporal resolution	Spatial extent	Distance (m)
DEMs	near-daily	39 x 5 m	0
PT sticks	3 days	30 sticks, 39 m	0
Bamboo forest	3-5 days	200 sticks, 200 m	~ 100
SSA sticks	daily	10 sticks, 90 m	~ 200
AWS PROMICE	daily	single point	~ 500

manual documentation indicates snowfall and the DEM data show an increase in surface heights, we consider this as snowfall.
This does, however, not exclude the possibility that snowdrift may have contributed to the increase. A negative change in snow
height is considered as depositional modification, which involves snowdrift, erosion, and re-distribution.

Surface roughness is often used to describe and analyse the size of landforms and features, and is therefore a useful tool
to investigate the variability in surface structures in our study area (Grohmann et al., 2011). We derive the surface roughness
following studies which analyse the surface variability with respect to a specific scale (van der Veen et al., 2009; Grohmann
et al., 2011; Veitinger et al., 2014). We use the peak to peak amplitude of 2.5 m long, non-overlapping segments following the
approach by Albert and Hawley (2002) and averaged individual values to a representative surface roughness estimate.

2.3 Accuracy estimates

We evaluated our DEMs by analysing the trueness of our DEM-derived snow height estimates compared to reference heights,
i.e., manually measured snow heights. For this, we first analysed the bias, i.e., the mean difference between DEM-derived
estimates and manually measured reference data. We further investigated the variability and dispersion as well as the overall
accuracy of our data by calculating the variance and the root mean square error (RMSE) between DEM-derived and manually
measured snow heights, respectively. Here, we report about two different evaluation schemes: 1) DEM-derived snow heights
around the locations of the PT sticks are compared to manually measured snow heights to assess the general data quality and
uncertainty in the study area; and 2) a sensitivity test on the number and dependency of GCPs by analysing DEM-derived and
manually measured reference snow heights from a second, independent validation area.

Data quality assessment

To assess the quality of DEM-derived snow height information, we compared manually measured data to DEM-derived snow
heights at the PT stick locations (for DEMs ±10 cm in x- and +10 cm in y-direction) for all days on which both data are
available (in total 14 days, see Table A1, Table B1 and Fig. B1). We consider the manually measured data as reference values,

i.e., the true snow heights. We find a mean difference of 0.28 cm, a variance of 0.28 cm^2, and a RMSE of 0.59 cm. Since manual data can be influenced by individual persons carrying out the measurement, for comparison we further analysed independent snow height estimates measured on the same day at the same locations by different people which resulted in a mean difference of 0.21 cm, a variance of 0.11 cm^2, and a RMSE of 0.39 cm, showing that the DEM RMSE of 0.59 cm is a conservative estimate.

Potential bias due to GCPs

GCPs are essential for a reliable geolocation of the DEMs. However, the final 3D model can be biased towards the fixed positions of the objects which are used as GCPs, resulting in a distortion or doming of the area (James and Robson, 2014). To assess possible biases, we set up a second, independent area outside of the surface science area with a size of 50 m^2 (10 m x 5 m, Fig. C1). This area was set up with the same procedure as the study area and was surrounded by 13 glass fiber sticks which were used as GCPs. Four additional sticks were distributed inside the area and used as an independent validation (*validation sticks*). Photos of this area were taken on 16th of June, 27th of June and 9th of July 2018. By comparing DEM-derived and manually measured snow height estimates at the validation sticks for all three dates, we obtained an overall mean difference of -0.32 cm, a variance of 1.65 cm^2, and a RMSE of 1.27 cm (Table C1). The accuracy is slightly lower with a higher RMSE than for our study area.

Furthermore, the validation sticks represent different snow heights and distances to the camera. Analysing these parameters in relation to the offset between DEM-derived and reference snow heights reveals no dependency on these factors (Appendix C).

Dependency on number and alignment of GCPs

As a final step, we evaluated the accuracy of our DEM-derived snow height estimates to the number of used GCPs. It is recommended to use at least three GCPs, however, more GCPs provide a better geo-referencing and a reduced sensitivity to a single point (e.g., James and Robson, 2012; Tonkin et al., 2016). We used the detailed snow height information from the validation sticks in the validation area and generated DEMs with five, eight or 13 GCPs. The mean differences between the DEM-derived and the manually measured snow heights at the validation sticks for the three days are 0.1 cm, -0.2 cm, and -0.3 cm, the variances are 2.38 cm^2, 2.30 cm^2, and 1.65 cm^2, and the RMSEs are 1.48 cm, 1.46 cm, and 1.27 cm, respectively (Appendix C). This analysis, however, assumes that all glass fiber sticks were vertically and horizontally precisely positioned, aligned in a straight line, and that all GCP marker positions were accurately set during the data processing. We therefore investigated these effects by purposely misaligning GCP positions at the top of the glass fibre sticks and adding randomly generated noise with a mean of 0 cm and a standard deviation of 2 cm to the marker coordinates. A scenario with inaccurate marker positions for the x-, y-, and z-coordinates results in a mean deviation of 0.08 cm, a variance of 0.97 cm^2, and a RMSE of 0.99 cm for the validation sticks (Table C3).

Uncertainties from manually setting up the transect, distributing the GCP coordinates during the processing, as well as the uncertainty of the GCP alignment are small, especially compared to the amplitude of snow height change throughout our

observation period (11 cm on average). We therefore conclude that our elevation models provide reliable snow height estimates
170   with a high enough accuracy for the purpose of our study.

3   Results

3.1   Relative snow heights from digital elevation models

Each of the 37 DEMs (Table A1, Fig. 3) represent a two dimensional map (39 x 5 m) of the relative snow height in the study
area for the particular day. The zero-point was chosen arbitrarily to be at the bottom of the first GCP on the day of installation.
175   All further snow heights are referenced to this zero-level.

On the first day of our observation period, 16th of May 2018 (hereafter we refer to the Day of Observation Period, *DOP*), the
snow height varied from -10.5 cm to +11.3 cm, with a total amplitude of 21.8 cm (Fig. 3 top panel). Two pronounced dunes were
present elongated along the prevailing wind direction and located in x-direction from ∼12 m to ∼20 m and around 32 m. Until
the middle of our observation period (20th of June 2018, DOP 36), the snow height has generally increased with a maximum
180   increase of 12 cm while the surface structures have changed slightly (Fig. 3 second panel). At the end of our observation period
(1st of August 2018, DOP 78), snow heights ranged from +2.6 cm to +16.4 cm, thus show a reduced amplitude of 13.8 cm
compared to DOP 1 (Fig. 3 third panel).

By comparing the DEMs between the beginning and the end of our observation period, we derived the change in snow height
throughout the 2018 spring and summer season (Fig. 3 fourth panel). This change amounts to an overall but not homogeneous
185   increase in snow height of ∼11 cm (10 and 90 % quantiles are 6.6 and 14 cm, respectively, Fig. 4a).

Over the season, the area affected by the manual snow sampling leading to missing DEM values is increasing. Thus, we
focus our main further analyses on an averaged band from y=2.5-3 m which is unaffected from the disturbances across the
entire season (Fig. 3 red bar in the top panel).

3.2   Comparison of different snow height estimates

190   To investigate the deviations of the snow height estimates as recorded by different methods and in different locations, we com-
pared our DEM-derived snow height data to other, independently obtained estimates (Table 1, Fig. 4b). Our photogrammetry
SfM approach indicates an increase in snow height of ∼11 cm from the first to the last day of available DEMs (Table 2 top row).
Manual measurements at the PT sticks showed an increase of 9.7 cm from DOP 5 to DOP 78. The Bamboo forest recorded an
increase in the snow height of 8.5 cm for the overlapping time period (DOP 10 to DOP 75). The SSA sticks showed an increase
195   of 10.9 cm (DOP 2 to DOP 78). Lastly, a snow height sensor mounted to the AWS PROMICE recorded an increase of 5.8 cm.
Note that since not every method was carried out every day, two different time intervals are considered. The observation of a
shorter period from DOP 10 to DOP 73 (to DOP 72 for the PT sticks and to DOP 71 for the Bamboo forest, Table 2 bottom
row) shows a smaller variation of snow height increases.
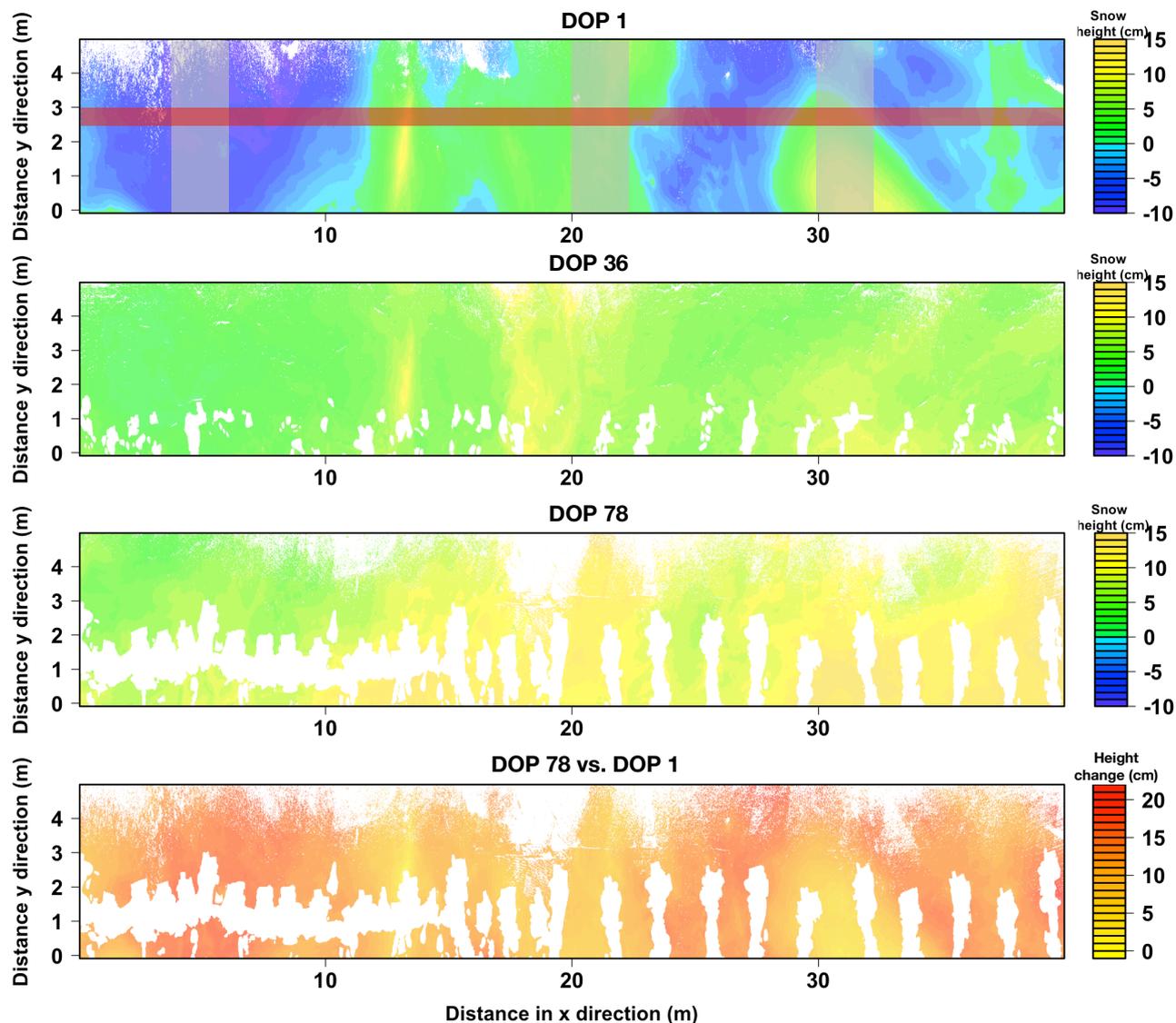
Figure 3. DEM-derived relative snow heights are presented as two dimensional maps (39x5 m). Snow heights for the Day of Observation Period 1 (16th of May 2018, DOP 1, upper panel), DOP 36 (20th of June 2018, second panel), and DOP 78 (1st of August 2018, third panel) are shown as well as the change in snow height between DOP 1 and DOP 78 (fourth panel). Snow height estimates are given in cm. The y-direction points towards the main wind direction. The zero-level refers to the position at x=0 m and y=0 m on the day of installation. The red bar (top panel) indicates a band along the x-direction of 50 cm width, which is used to obtain average snow heights for each day for further analyses. The grey bars mark three subareas for further analyses. Missing data are shown as white areas and are caused either by a snow sampling scheme performed in the same area (white spots close to the lower main line) or by insufficient image quality.

Table 2. Snow height changes for the different snow height estimates (Table 1) throughout the observation period. Changes are given in cm. Two different periods are considered to include first the entire observation period covered by the DEMs (i.e., DOP 1 to 78) and second to compare the most common time interval, especially for the PT sticks and the Bamboo forest (temporal resolutions are mentioned in Table 1).

Name	DEM	PT sticks	Bamboo forest	SSA sticks	AWS PROMICE
DOP	1 - 78	5 - 78	10 - 75	2 - 78	1 - 78
Change (cm)	11	9.7	8.5	10.9	5.8
DOP	10 - 73	11 - 72	10 - 71	10 - 73	10 - 73
Change (cm)	10.3	10.7	8.5	10.9	7.6

Despite differences in the amount of snow height increase (Fig. 4a), the individual estimates agree on the overall temporal evolution (Fig. 4b). The increase in snow height, however, does not occur continuously and uniformly. The development over time is much more characterised by a few individual, large events, such as the event around DOP 21 that led to an increase of ∼5 cm.

Manual documentation of snowfall (Table A1) contains only the information when snowfall occurred, but no indication on the amount. By contrast, all snow height estimates show only the total snow accumulation including depositional changes such as snowdrift and re-distribution, but not the net amount of snowfall during a single event. Thus, we compared the ERA5 snowfall product to our manual documentation (Fig. 4c). Both our manual documentation and the ERA5 product agree in general well on the timing of snowfall, while the ERA5 snowfall product provides additional information on the varying amounts of snow. Moreover, a comparison of the ERA5 product with all individual snow height estimates from Fig. 4b shows agreement for the event around DOP 21. The many smaller events between DOP 30 and DOP 60 seem to constitute the gradual height increase in the observations. ERA5 further indicates snowfall on days without a manual note of snowfall which can be due to many reasons, for example snow during the night which was not documented, snow which was directly blown away and did not deposit on the surface at all, or inaccuracies of ERA5.

3.3 Day-to-day variation and the erosion of fresh snowfall

To visualise snow accumulation and removal, we analysed ten available DEMs from the beginning of our observation period (DOP 1 to DOP 12, Fig. 5). The mean snow height increased by 4.1 cm from the first to the fifth day which is consistent with manually documented snowfall. The ERA5 snowfall product agrees in the timing of snowfall (Fig. 4c, Table A1), but not regarding the amount (0.6 cm). The DEM-derived snowfall increase is evenly distributed across the troughs and dunes. In contrast, the subsequent decrease in snow height from DOP 7 to DOP 8 (-3.6 cm) is more variable along the study area. The end of this twelve-day period shows erosion of snow (mean snow height change of -0.5 cm) and an exposure of the initial surface structure from the first day which might have been caused by higher wind speeds on DOP 11 and DOP 12 (Fig. A1).

To investigate the erosion and the repeated exposure of previous surface structures across the full time period, we analysed the RMSE between the snow surface height from one fixed day compared to all other days (Fig. 6). We use this measure as an
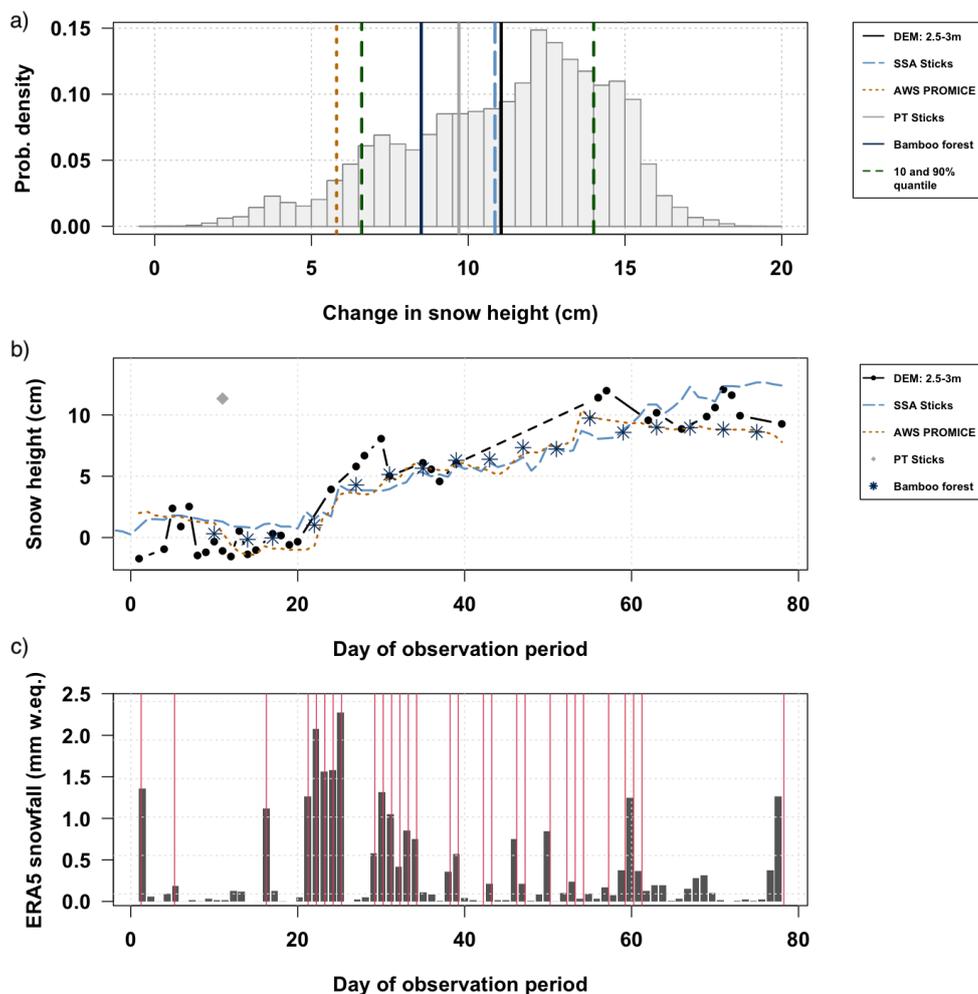
Figure 4. Evolution and changes of different snow height estimates throughout the observation period. a) Histogram of the change in snow height for every single pixel (resolution of 1 x 1 cm) of the DEMs from DOP 1 to DOP 78 (Fig. 3 fourth panel), as well as the estimated changes in snow height from other methods (Tables 1 and 2). Note that the single line estimates cover different spatial extent. The SSA Sticks are an average of ten sticks across 90 m. The AWS PROMICE is a daily average of a single point, high-resolution measurement from a sonic snow height sensor. The PT Sticks are an average of 30 manual measurements along the photogrammetry area. The Bamboo forest is an average of 200 sticks across 200 m. The DEM line is the average of a horizontal band from 2.5 m to 3 m in y-direction (Fig. 3 red bar). b) Estimates of the relative snow height throughout the observation period from the DEMs, the SSA Sticks, the AWS PROMICE, the PT Sticks, and the Bamboo forest. For a direct comparison, each estimate is referred to its mean value across DOP 10 to DOP 20, which is defined as the zero level. c) The ERA5 snowfall product for the observation period. Red lines indicate manually documented snowfall (Table A1).

indicator of how similar or different the snow surface structure is during our observation period. Therefore, the erosion of snow leading to the exposure of previous surfaces is visible as a local decrease of the RMSE. Similar behaviour as shown in the case
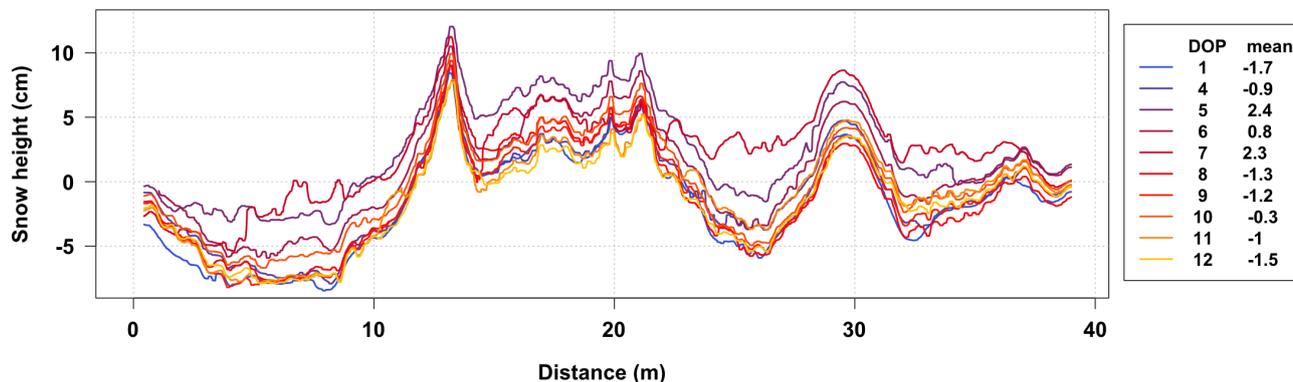
Figure 5. Relative horizontal snow height profiles (20-point running median, averaged in y-direction from 2.5 to 3 m). Different colours represent different days from DOP 1 to DOP 12 as well as respective mean snow heights in cm, both shown in the legend. Snowfall caused an overall snow height increase from DOP 1 to DOP 7, followed by an erosive event removing the new snow, and exposing the previous surface structure again.

225 study in Fig. 5 visible as local peak in the RMSE between DOP 5 and DOP 10 (black) occurs again between DOP 28 and DOP 31 as well as between DOP 70 and DOP 73. This suggests that the build-up and erosion of surfaces is a common feature at the study site.
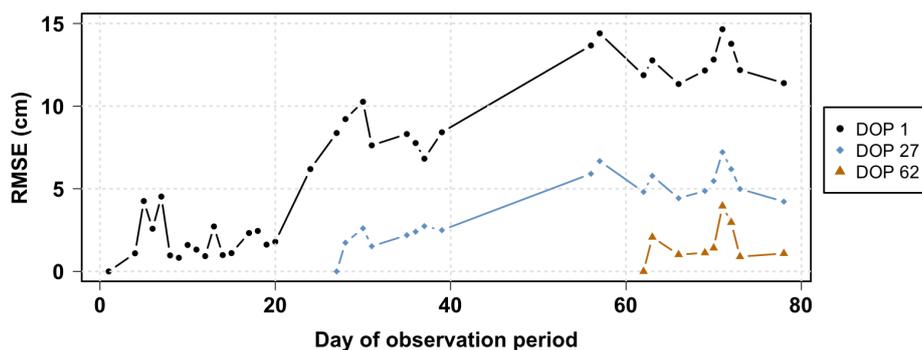
Figure 6. Root mean square error (RMSE) between the transient surface structures and the surface structures of three reference days: DOP 1 (black), DOP 27 (blue), and DOP 62 (gold). Low values indicate days with similar, high values days with dissimilar surface structures compared to the reference day.

3.4 Relationship between initial snow height and snow accumulation

We have seen that the snow surface became flatter towards the end of our observation period (Sect. 3.1). We therefore studied
230 the change of the snow height between DOP 1 and DOP 78 and investigated the relationship between the relative snow height
and the amount of accumulated snow.

First, we analysed the area perpendicular to the main wind direction and observed a change from a heterogeneous to a more
homogeneous snow surface (Fig. 7a). We then studied the behaviour of the snow surface parallel to the wind direction for three
selected subareas with different initial surface structures (grey areas in Fig. 3 upper panel). The snow structures in these areas
235 were characterised on DOP 1 by a trough (area from 4 to 6 m), the top of a dune (area from 20 to 22 m), and an undulating
surface (area from 30 to 32 m, Fig. 7b dotted lines). While the first and second subareas received a very homogeneous snow
accumulation of ∼14 and ∼6 cm, respectively, the third subarea received a variable amount of snow accumulation such that
the partial dune undulation present at DOP 1 has nearly vanished at DOP 78. Thus, despite the differences at the beginning of
the observation period, all three subareas developed to similar relative snow heights on DOP 78 (Fig. 7b solid lines).
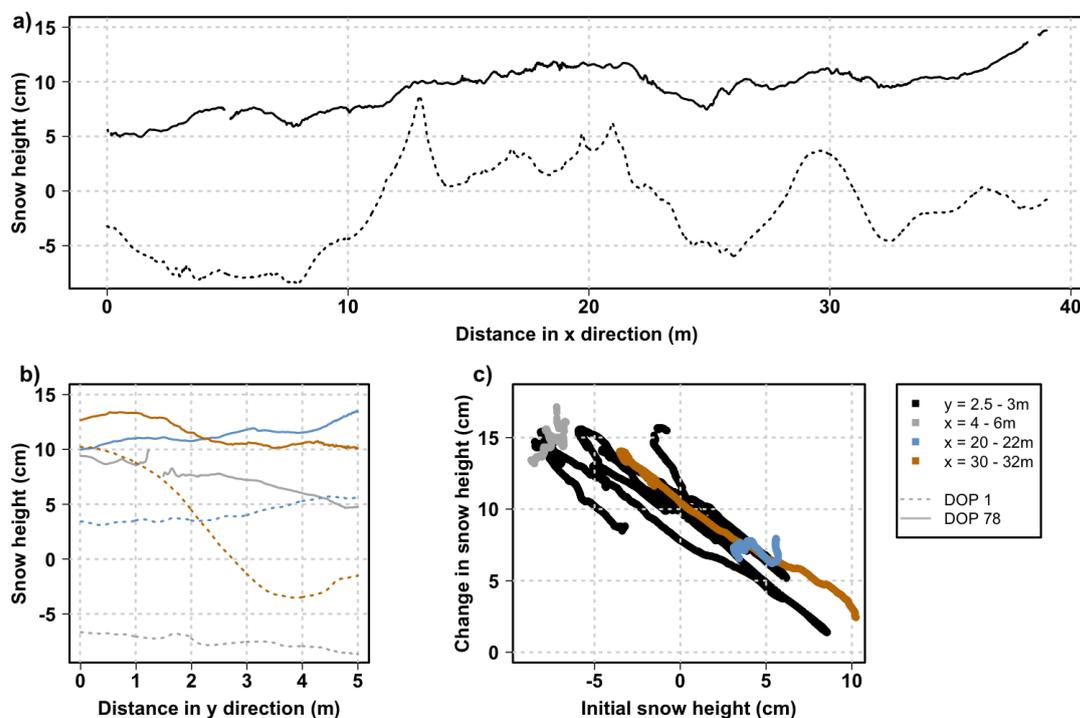
Figure 7. DEM-derived snow heights for 16th of May (DOP 1, dotted lines) and 1st of August, 2018 (DOP 78, solid lines) for four subareas
of the study area: a) the averaged band in y-direction; b) three subareas parallel to the main wind direction (grey: 4 m to 6 m, blue: 20 to 22 m,
and gold: 30 to 32 m). These subareas are marked with grey bars in Fig. 3. c) The relationship between the initial snow height on DOP 1 and
the change in snow height to DOP 78 is shown. Note that the legend refers to all panels.

240   Using these data, we can infer a relation between the initial snow height and the change in snow height, i.e., the amount of accumulated snow. More specifically, we find a strongly negative correlation (Fig. 7c) indicating that areas which started with a relatively high snow height received less snow while areas with a comparably low initial snow height received more accumulation.

3.5   Surface roughness

245   We analysed the surface roughness perpendicular and parallel to the main wind direction by using the peak to peak amplitude of 2.5 m long, non-overlapping segments along the y=2.5 m line and from y=1 m to y=3.5 m in 50 cm steps along the x-axis, respectively. Individual estimates are averaged to a daily estimate perpendicular and parallel to the main wind direction. The extent for estimates parallel to the main wind direction was chosen in order to be least affected by sampling locations and missing values towards y=5 m. However, it is likely to be less accurate due to the increasing lack of data at the snow sampling

250   positions towards the end of the observation period.

    We found a consistent decrease in surface roughness from ~4 cm to ~2 cm in both directions (Fig. 8). We are unfortunately missing data between DOP 40 and DOP 56, a period during which the surface roughness seems to increase after a decreasing trend from DOP 20 to DOP 38. Moreover, the surface roughness estimate parallel to the main wind direction shows a smaller overall change than the estimate perpendicular to the main wind direction.
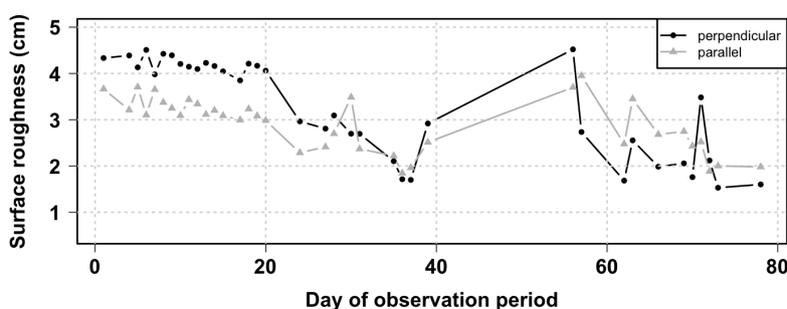
Figure 8. Surface roughness estimates throughout the observation period following the method from Albert and Hawley (2002). Estimates are based on 2.5 m long, non-overlapping segments along the y=2.5 m line perpendicular to the main wind direction (black) as well as from y=1 m to y=3.5 m for estimates parallel to the main wind direction (grey). The individual estimates, perpendicular or parallel to the main wind direction, are averaged to a representative surface roughness.

4 Discussion

4.1 Photogrammetry SfM as an efficient snow surface monitoring tool

We showed that our close-range photogrammetry SfM approach delivers reliable snow height information with an accuracy of ∼1.3 cm. The method can be used to characterise the spatio-temporal snow evolution on a decimetre to 100 m spatial scale with a daily resolution. Our setup has several advantages in contrast to alternative approaches. Compared to single point measurements, we benefit from spatial information encompassing an area of 195 m^2. Previous laser scanner studies covered areas of only 40 m^2 and 110 m^2 and can only be extended by placing the laser higher above the ground (Picard et al., 2016, 2019). Our approach offers the flexibility of repeatedly covering a spatial scale with specific desired dimensions (e.g., an area with a length of 100 m) and orientations. In contrast, this is not possible for a laser scanner that is fixed in one position with a specific radius, or for manual point measurements, sonic snow height sensors or ground penetrating radar (Basnet et al., 2016; Cimoli et al., 2017).

Furthermore, our approach does not require expensive equipment, as all the necessary items for image acquisition are commercially available. The method can be easily operated in remote areas and the logistical effort is low. It does not require a permanent power supply, which can be a limiting factor for laser scanners and snow height sensors. No specific training for users is needed as is required for airborne studies with aircraft (e.g., Baltsavias et al., 2001), drones (e.g., Hawley and Millstein, 2019) or LiDAR operations (e.g., Deems et al., 2013). Even though our approach is limited by light availability and visual contrasts, which is also reported in many studies (e.g., Nolan et al., 2015; Harder et al., 2016; Cimoli et al., 2017), it has the advantage of being very easy to operate and that it can be used at other study sites without great effort.

Since this study was the first time the setup was used, missing days were the result of human error. To improve future studies, we suggest to use an infrared filter to enhance the image quality and facilitate data acquisition even during cloudy and bad weather conditions (Bühler et al., 2015; Adams et al., 2018). Furthermore, placing the camera higher above the ground could enhance the spatial coverage (Picard et al., 2019).

4.2 Reliable determination of snow accumulation

Typically, a snow height sensor integrated in an AWS delivers high temporal resolution data for only a single point and measures the accumulation at one specific location on an ice sheet. Our results show that at least at our study site, such a single point measurement would not deliver spatially representative information on a seasonal timescale. If only a single point in our study area was chosen, it would result in a snow accumulation estimate for our study period that would vary between 6.6 and 14 cm (10 and 90 % quantiles, Fig. 4a). The AWS PROMICE estimate is at the edge of this range (5.8 or 7.6 cm depending on the selected time period, Table 2) and deviates from the average snow height change of ∼11 or 10.3 cm, respectively, determined by the photogrammetry SfM method.

Accumulation estimates from snow stake farms and grids are averaged over multiple sites and are thus more representative (Kuhns et al., 1997; Eisen et al., 2008), but the remaining uncertainty will depend on the number and spacing of the stakes (Laepple et al., 2016; Münch et al., 2016, 2017). We can test this dependency based on our spatio-temporal data set. By

simulating the sampling from different stake setups and comparing it to the accumulation estimate from the full DEM data set,
the root mean square deviation (RMSD) of the extracted mean snow height change relative to the overall mean shows a clear

290 dependency on the choice of the distance between the sampling points (Fig. 9). Averaging ten sampling points (equivalent to
stakes) with a one metre distance results in a similar error on the accumulation estimate as using only two sampling points
with a larger (5 or 10 m) distance. This effect can be explained by the typical size of surface structures, on the scale of several
metres at our study site. Sampling the same feature multiple times does not increase its representativeness, whereas sampling
points far enough apart to avoid the same feature, contains more information. Thus, for study sites similar to EGRIP, a setup

295 to reliably derive snow accumulation with a RMSD <1 cm using sticks could for example consist of either 25 sticks with 1 m
distance or seven sticks with 5 m distance.
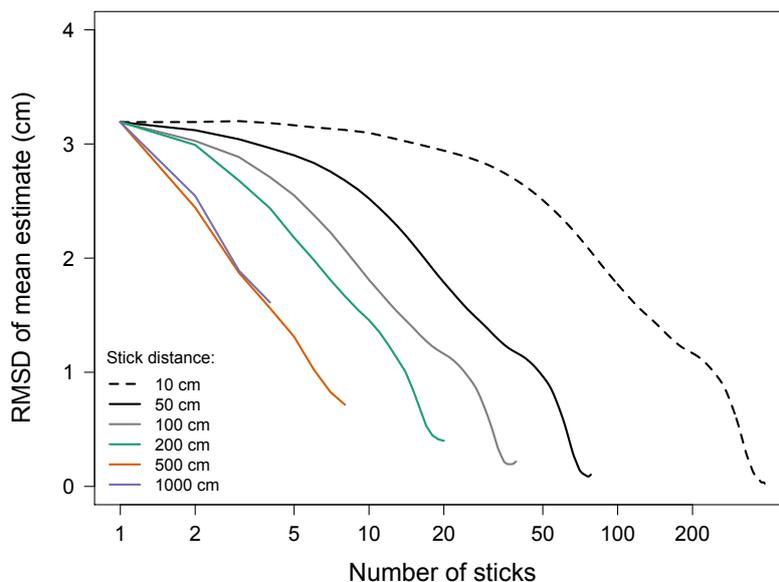
Figure 9. The uncertainty of the estimated mean snow height change as a function of the number of sampling points ("sticks") and the
distance between them. The mean snow height change is calculated from the DEM data at y=2.5 m for all possible sequences along the
x-direction which consist of N sampling points with a given distance from one point to the next. The figure shows the RMSD between the
mean snow height change of the respective sequences and the mean snow height change as calculated using all available sampling points.

4.3 Temporal and spatial change of surface structures

The snow surface changed considerably throughout our observation period. For example, the surface roughness decreased from
around 4 to 2 cm (Fig. 8). An increase of surface roughness in winter, followed by a decrease in summer, is often attributed to

300 seasonally changing wind speeds, with higher wind speeds in winter (e.g., Albert and Hawley, 2002). Our observed decrease
in surface roughness towards summer is comparable to results from a laser altimetry study covering a large area of central and

northern parts of the Greenland ice sheet (van der Veen et al., 2009) and to a study from Summit, Greenland, with a similar spatial extent (Albert and Hawley, 2002). Wind speed thresholds for event-driven snow deposition and drift are reported to be $4\,\text{m}\,\text{s}^{-1}$ for a 100 hour average at 3 m above the surface, or higher wind speeds for a shorter time period, called gust

305 (Groot Zwaaftink et al., 2013). At our study site, the winter wind speed is generally higher than the summer wind speed and exceeds the proposed threshold values (not shown here). Lower summer wind speeds can therefore explain the observed decrease in surface roughness.

In accordance with a decreasing surface roughness, our data further show distinct undulations at the beginning of our observation period, which develop into a rather flat surface towards the end of our observation period (Figs. 3, 7a and 7b). The

310 flattening is characterised by a negative correlation between the initial snow height and the local accumulation (Fig. 7c), and thus in the long-term, also between the accumulation from one year to the next. The process of building up and wearing down of surface undulations is reported for many different locations on large ice sheets (Gow, 1965; Albert and Hawley, 2002; Groot Zwaaftink et al., 2013; Laepple et al., 2016). This process further implies that local deviations from the mean accumulation rate will quickly average out over time as they cancel each other out (Fisher et al., 1985). It further explains why

315 accumulation estimates from firn or ice cores that only sample one point but average across a large time-window, provide a good estimate of the regional accumulation rate, as already suggested by Kuhns et al. (1997) and van der Veen et al. (2009).

Our results further demonstrate that high erosion rates of the surface snow are not random in space and time, but instead are able to remove an entire snowfall event and uncover an older surface (Figs. 5 and 6). Unfortunately, our current data set is too short and does not provide micro-scale properties of the snow to detect which conditions favour the fixation of the snow

320 surface and thus its long-term preservation, or to render it unstable enough to be eroded.

The mean snow height increase derived from our photogrammetry SfM approach was ∼11 cm in our study area. The total amount of snow input into our area was, however, more than 30 cm considering only the positive contributions from precipitated and drifted snow (Fig. 10). The observed accumulation corresponds only to ∼35 % of the total amount of temporarily deposited snow emphasising the substantial contribution of snowdrift and snow re-distribution to the final snow accumulation.

325 Converting the ERA5 snowfall product from mm w.eq. to cm of snow (using a density of $290\,\text{kg}\,\text{m}^{-3}$ obtained from daily density measurements on site) results in ∼8 cm of net snowfall (Fig. 10). This result suggests that the build-up of the snowpack is very irregular in time, resulting not only from the precipitation intermittency itself (Persson et al., 2011), but also from intermittent depositional modifications. This overall accumulation intermittency can significantly influence the recording of climate proxies in the snow and firn, as e.g., local climate signals preserved in the snow can either be removed locally by transport to other

330 locations or in turn be derived from other locations through re-deposition.

To visualise the overall accumulation intermittency in the surface snow, we created a 2D snowpack (Fig. 11) by considering snow height increases from one day to the next as positive contributions, and decreases in snow height as snow erosion, which removes previously deposited layers. The sequence and different thickness of temporal, i.e., coloured, layers indicates that some snowfall or snowdrift events are larger and/or more preserved than others. For example, the strong event on DOP 21 is

335 present with a thick layer and seems therefore to be fully preserved, while smaller events (e.g., on DOP 58, Fig. 4) are not preserved. We note that some layers might be influenced by the temporal resolution of our data set. However, this does not
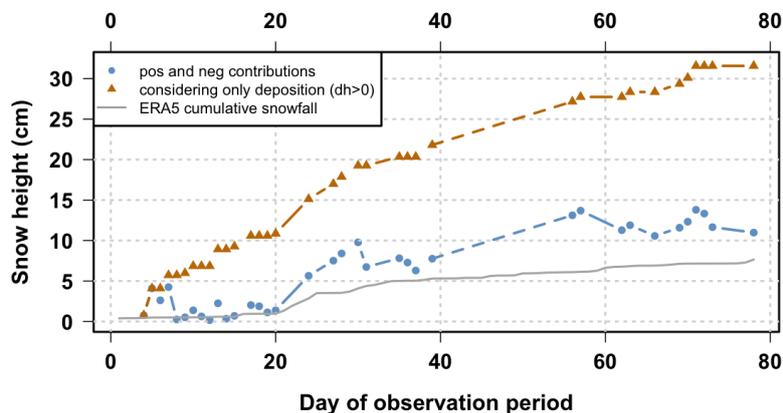
Figure 10. Cumulative snow height over the observation period from DEM-derived data and from the ERA5 reanalysis snowfall product. The DEM-derived snow height is shown for the two possibilities of i) counting both positive and negative contributions from one day to the next (blue), and ii) counting only the positive contributions (gold). The ERA5 snow height (grey) is based on the reanalysis snowfall product converted from mm w.eq. to cm assuming a mean snow density of $290 \, \text{kg m}^{-3}$. Considering only the positive changes in the DEM-derived data accounts for deposition by snowfall or drift, but not for snow removal by e.g., erosion. This indicates that more than half of the snow that arrived at the study site was eroded and re-distributed again, and was thus transported out of our study area. The ERA5 snowfall product indicates less direct snowfall than recorded by the DEMs.

apply to the mentioned layer on DOP 21 (orange area in Fig. 11) and to the missing layer around DOP 58. Thus, our analysis suggests that the internal structure is characterised by only a small number of events with varying layer thicknesses and a large internal heterogeneity in snow age, both in space and time.

4.4 Implications for the interpretation of proxy data

Our results have several implications for the interpretation of climate proxies in firn and ice such as stable water isotopologues. They demonstrate the importance of precipitation intermittency, address the uncertain spatio-temporal representativeness of local snow accumulation, and show the non-local behaviour of depositional modifications on the snow surface.

Our data indicate that the internal structure of the snow column is dominated by a small number of events (Fig. 11), which suggests that a firn or ice core does not record every precipitation event. The large heterogeneity in accumulation rate and the depositional modifications of the snow surface imply that at sites with similar conditions parameters measured in a single firn core will not be representative on a seasonal scale (e.g., Fig. 2 from Masson-Delmotte et al., 2015). This pattern is not only due to precipitation intermittency, a factor often considered in the interpretation of paleoclimate records (Persson et al., 2011; Sime et al., 2011; Casado et al., 2018), but also due to the erosion of snow layers. We refer to the interplay of both processes as accumulation intermittency. This process will create a strong noise level due to an under-sampling of the continuous environmental signal (Casado et al., 2019) and also lead to the possibility that a singular event, such as a singular deposition of
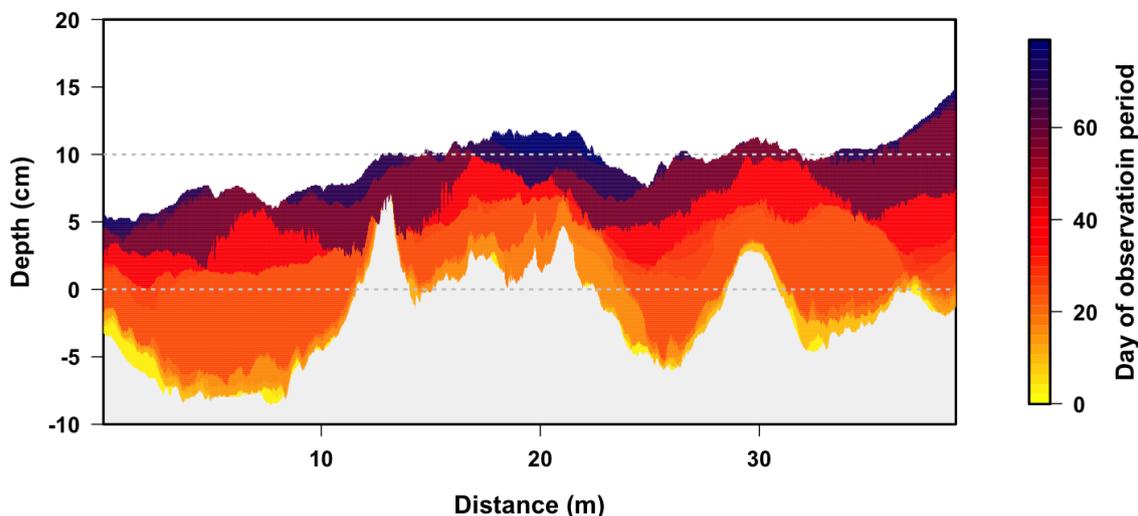
Figure 11. Two-dimensional view of the internal structure of our study area along the x-direction on the last day of our observation period (DOP 78) estimated from the DEM-derived data. Colours indicate the day of deposition during the season, namely when the snow height increased at the respective location. The light grey area represents the surface undulations prior to our first DEM. The longest data gap is between DOP 39 and DOP 56 (Table A1) which, however, does not cause an unrealistically thick snow layer, showing that the temporal resolution of our data set does not strongly influence the internal layering derived here.

a proxy signal from a volcano or a biomass burning peak, might be missed. If erosion is not random, but instead depends on climatic conditions such as the season (Albert and Hawley, 2002), this might also bias the recorded signal. Further longterm observations of the precipitation vs. accumulation statistics (Picard et al., 2019) and spatial studies of the signal recorded in

355   snow and firn (Münch et al., 2016, 2017) will help to better quantify this effect and allow for a more reliable interpretation of proxy data from firn and ice cores.

Furthermore, surface roughness in combination with wind may lead to the ventilation of the upper snow and possibly influence the depth of the ventilation (Albert and Hawley, 2002); i.e., the rougher the surface, the deeper the ventilation (Fisher et al., 1983). Our findings that greater surface roughness occurs towards spring, may indicate a stronger exchange between

360   the snow surface and the atmosphere during winter and spring compared to summer. However, stronger exchange is expected during summer due to higher temperatures, higher moisture availability, and thus higher fluxes.

The strong difference between the total snow input and the net accumulation suggests that snow transport and thus a re-location of the climate signal might also influence the recorded signal. For signals with strong spatial variations such as stable water isotopologues, these processes might be able to distort the local climate signal. Unfortunately, our data set does not allow

365   to quantify the degree of wind scouring or to infer the spatial extent of the snow transport and the initial location of a re-located climatic signal. We therefore cannot determine the amount of mixing of climatic signals.

To better constrain the effects of accumulation intermittency on the preserved climatic information, a combination of snow height information derived from our photogrammetry SfM approach and the collection of proxy data (e.g., stable water isotopologues) from the same area can help to better understand the relationship between accumulation intermittency and preserved

370   climatic information. Compared to single point measurements, our spatial data set has the advantage of being better able to evaluate the re-distribution and final settlement of snow. However, determining the origin and composition, e.g., the homogeneity, of drifted snow and associated imprinted climatic signals, is essential but still challenging. Measuring the proxy signal at different stages during the deposition process, i.e., freshly precipitated snow, surface snow during vapor exchange with the atmosphere, drifted snow, and buried snow, and combining these data with DEM-derived snow height information, will help to

375   close the gap between the climatic information and the proxy signal.

5   Conclusions

We presented high-resolution elevation models of the snow surface evolution at the EGRIP campsite in northeast Greenland using a novel photogrammetry SfM approach. This method delivers snow height information on the decimetre to 100 m scale with an accuracy of ∼1.3 cm. The derived data set covers a three-month period from May to August in 2018, which experienced

380   an overall snow height increase of ∼11 cm.

A comparison of the snow height evolution based on our DEM-derived data to other snow height estimates from single or multi-point measurements shows a similar trend in the overall snow height evolution. Moreover, the snow height increase is not linear but rather characterized by fluctuations due to intermittent snowfall and wind-driven erosion. This is shown by day-to-day changes in our data indicating an increase and subsequent decrease in the snow height caused by snowfall and snow

385   erosion, respectively. These variable accumulation patterns result in an internal spatial and temporal heterogeneity of snow age and layer thicknesses.

Our data set further recorded the transition from a rough winter to a flat summer snow surface throughout our observation period, with a decrease in surface roughness from 4 to 2 cm towards the summer. This is also seen in a negative relationship between the initial snow height and the amount of accumulated snow. Surface structures such as dunes and sastrugi are therefore

390   intermittent and not preserved from year to year.

Proxy data from ice cores are typically interpreted as precipitation-weighted signals. However, we showed that there are significant differences between precipitation and accumulation and that depositional modifications considerably change the structure of the snow surface. Investigating the dependency of proxy signals on the surface structures and on the general depositional processes leading to the signal imprint at different locations would therefore enhance the understanding and

395   interpretability of proxy records.

Data availability. The photogrammetry SfM data are available in the PANGAEA data base (https://www.pangaea.de) under https://doi. pangaea.de/10.1594/PANGAEA.923418, the SSA stick data are available under https://doi.pangaea.de/10.1594/PANGAEA.921853, and the

Bamboo forest data under https://doi.pangaea.de/10.1594/PANGAEA.921855. The PT Stick data are submitted to the PANGAEA data base and the final DOI will be provided once it is available. Data from the Programme for Monitoring of the Greenland Ice Sheet (PROMICE)

400 were provided by the Geological Survey of Denmark and Greenland (GEUS) at http://www.promice.dk.

Appendix A: Additional meteorological and photogrammetric information
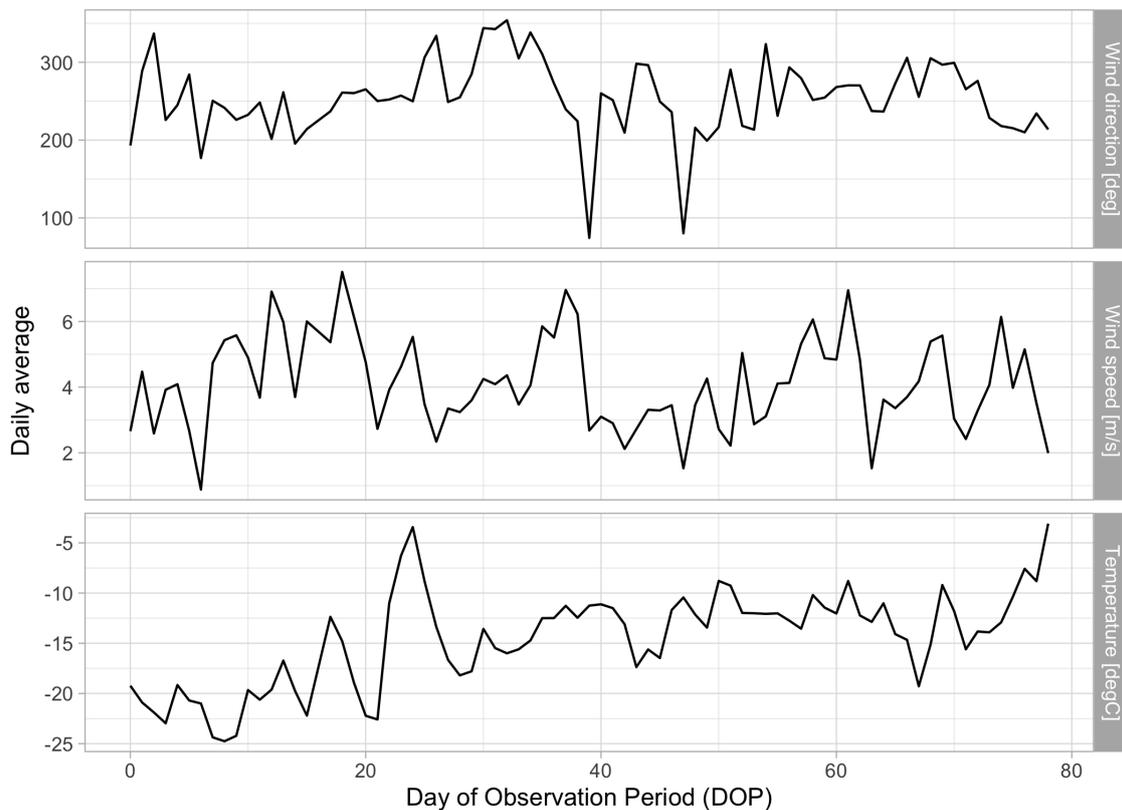
Figure A1. Daily averages of meteorological parameters, i.e., wind direction in [°], wind speed in [m s^{-1}] and air temperature in [°C], measured at 2 m height at the AWS PROMICE for the observation period from 16th of May (DOP 1) to 1st of August 2018 (DOP 78).

Table A1. Detailed information on the fieldwork campaign, including Day of Observation Period (DOP), Day Of Year (DOY), the date, the availability of a DEM, manual snow height measurements at the PT sticks (PT), and manually documented snowfall. We refer to day of observation period in the text, in figures and tables.

DOP	DOY	Date	DEM	PT	Snowfall	DOP	DOY	Date	DEM	PT	Snowfall
1	136	16.05.2018	x		x	40	175	24.06.2018			
2	137	17.05.2018				41	176	25.06.2018		x	
3	138	18.05.2018				42	177	26.06.2018		x	x
4	139	19.05.2018	x			43	178	27.06.2018		x	x
5	140	20.05.2018	x	x	x	44	179	28.06.2018		x	
6	141	21.05.2018	x			45	180	29.06.2018			
7	142	22.05.2018	x			46	181	30.06.2018			x
8	143	23.05.2018	x	x		47	182	01.07.2018		x	x
9	144	24.05.2018	x			48	183	02.07.2018			
10	145	25.05.2018	x			49	184	03.07.2018		x	
11	146	26.05.2018	x	x		50	185	04.07.2018		x	x
12	147	27.05.2018	x			51	186	05.07.2018			
13	148	28.05.2018	x			52	187	06.07.2018			x
14	149	29.05.2018	x	x		53	188	07.07.2018			x
15	150	30.05.2018	x			54	189	08.07.2018		x	x
16	151	31.05.2018			x	55	190	09.07.2018			
17	152	01.06.2018	x	x		56	191	10.07.2018	x		
18	153	02.06.2018	x			57	192	11.07.2018	x	x	x
19	154	03.06.2018	x			58	193	12.07.2018			
20	155	04.06.2018	x			59	194	13.07.2018		x	x
21	156	05.06.2018		x	x	60	195	14.07.2018			x
22	157	06.06.2018			x	61	196	15.07.2018		x	x
23	158	07.06.2018		x	x	62	197	16.07.2018	x		
24	159	08.06.2018	x		x	63	198	17.07.2018	x		
25	160	09.06.2018			x	64	199	18.07.2018			
26	161	10.06.2018		x		65	200	19.07.2018			
27	162	11.06.2018	x			66	201	20.07.2018	x	x	
28	163	12.06.2018	x	x		67	202	21.07.2018			
29	164	13.06.2018			x	68	203	22.07.2018			
30	165	14.06.2018	x	x	x	69	204	23.07.2018	x	x	
31	166	15.06.2018	x		x	70	205	24.07.2018	x		
32	167	16.06.2018			x	71	206	25.07.2018	x		
33	168	17.06.2018		x	x	72	207	26.07.2018	x	x	
34	169	18.06.2018			x	73	208	27.07.2018	x		
35	170	19.06.2018	x			74	209	28.07.2018			
36	171	20.06.2018	x	x		75	210	29.07.2018		x	
37	172	21.06.2018	x			76	211	30.07.2018			
38	173	22.06.2018			x	77	212	31.07.2018			
39	174	23.06.2018	x	x	x	78	213	01.08.2018	x	x	x

Appendix B: Ground control analysis for the study area

The difference between the DEM-derived snow heights and the reference data (i.e., manually measured snow heights at the PT sticks) is used to assess the accuracy of the photogrammetry SfM technique. DEM-derived snow heights at the locations of the PT sticks (± 10 cm in x- and $+10$ cm y-direction) are compared to the manually derived snow heights for all days on which both data are available (Table A1). Mean differences, variances, and root mean square errors (RMSE) are listed in Table B1 and the mean difference is further illustrated in Fig. B1. Marker accuracies were determined by a manual check of the alignment in the processing software Agisoft PhotoScan (Fig. C1b and c). Note that some estimates in Table B1 are based on less than 30 data points due to missing data caused by the snow sampling.

Table B1. Accuracy estimates for DEM-derived snow heights in our study area. Mean differences, variances, and RMSEs between DEM-derived snow heights for the areas around the PT stick locations (± 10 cm in x- and $+10$ cm in y-direction) and manual snow height measurements are listed. Data are given for all days of the observation period (DOP) on which both DEM-derived and manually measured snow heights are available (Table A1).

DOP	5	8	11	14	17	28	30	36	39	57	66	69	72	78
Mean difference (cm)	0.35	-0.92	-0.02	-0.75	0.11	0.84	0.64	0.17	0.36	0.68	-0.15	0.37	0.93	0.23
Variance (cm^2)	0.93	0.75	1.47	0.49	0.79	2.35	3.98	0.62	1.55	1.47	1.52	1.94	1.76	1.95
RMSE (cm)	1.01	1.25	1.19	1.00	0.88	1.73	2.06	0.79	1.27	1.37	1.22	1.42	1.60	1.39
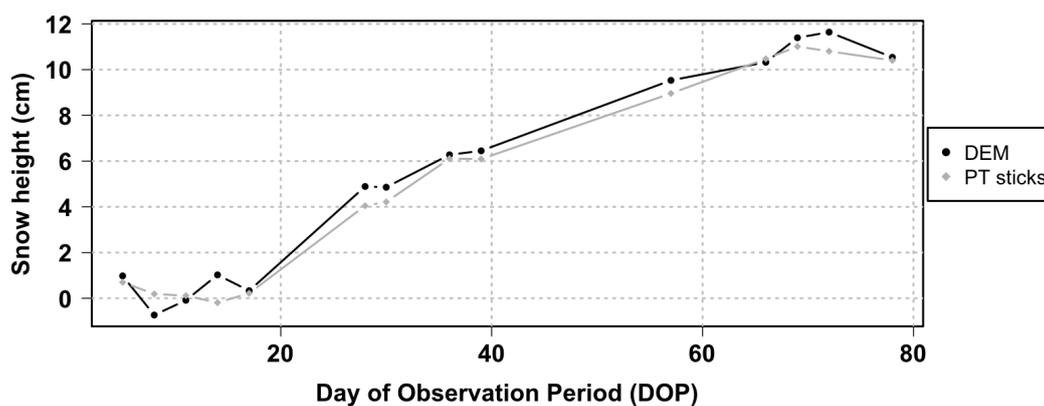
Figure B1. DEM-derived snow heights for the areas around the PT stick locations (± 10 cm in x- and $+10$ cm in y-direction, black) and manually measured snow heights (grey). Presented are data for all days during the observation period (DOP) on which both DEM-derived and manually measured snow heights are available (Table A1).

Appendix C: Validation

The quality of the DEMs can be affected by many aspects during the image acquisition, the GCP allocation, and the DEM processing. During the image acquisition, the camera resolution, the camera-to-object distance, and the angle of the camera towards the surface can influence the quality of the images (Basnet et al., 2016). Moreover, the introduction of GCPs is necessary to generate geo-referenced DEMs. However, the models can be biased towards the fixed positions of the GCPs, i.e., the glass fibre sticks, due to a stronger contrast (Fig. C1b and c) (e.g., Cimoli et al., 2017). Since GCPs are only distributed on the edge of the study area, a detailed analysis on potential biases, such as doming effects inside the area, was performed. Further, human mistakes during the aligning of the sticks as well as misalignments of GCP marker points during the processing in Agisoft PhotoScan can introduce additional uncertainties and are investigated here.

Ground control analysis for the validation area

A validation area was set up outside of the surface science area but with the same procedure as the main study area. The walking side was marked with eleven glass fibre sticks with 1 m-spacings (x=10 m). Two additional sticks were placed to the right and left side with 5 m distance to the main line (y=5 m, total area of 50 m^2, Fig. C1a). Four additional sticks (hereafter called *validation sticks*) were distributed inside the area on different local snow structures and with different distances to the main line. Image acquisition of this area was performed on three days to account for varying uncertainties in time (Adams et al., 2018). Photos were taken on 16th of June with very bright light conditions, and further on 27th of June and 9th of July 2018 with suitable weather conditions. The snow surfaces were very different on these three dates with a very flat and smooth surface, the presence of frost and rime, and small ripple structures, respectively. To not disturb the DEM generation, the manual snow height measurements at the validation sticks were performed after the image acquisition. Accuracy estimates derived from the mean difference, the variance, and the RMSE between DEM-derived and manually measured snow heights at the validation sticks were lowest on 9th of July and highest on 27th of June 2018 (Table C1). Neither the photos nor the DEMs provide a clear explanation for these differences.

Table C1. Accuracy measures for the validation area. Mean differences, variances, and RMSEs between DEM-derived and manually measured snow heights are presented for the validation sticks in the validation area.

Date	16.06.2018	27.06.2018	09.07.2018
Mean difference (cm)	0.71	-1.73	0.04
Variance (cm^2)	0.45	0.61	0.74
RMSE (cm)	0.92	1.86	0.74
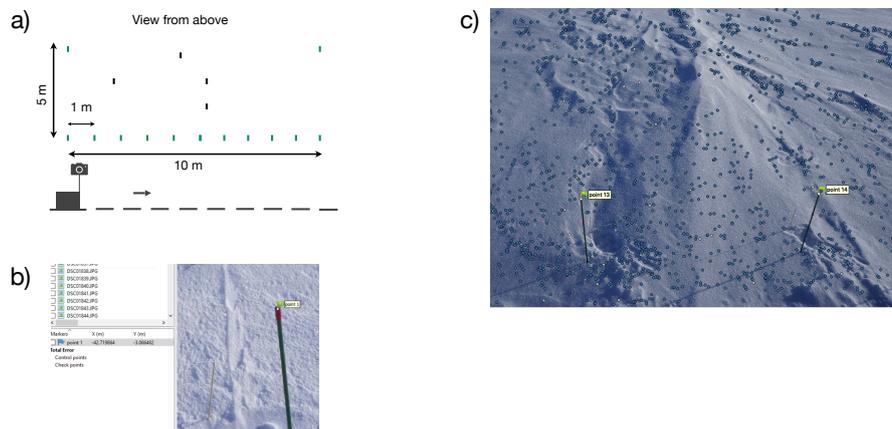
Figure C1. Validation area and possible error sources during the processing workflow. a) Schematic illustration of the validation area which was set up according to the same procedure as the main study area but outside of the surface science area. 13 glass fibre sticks were distributed (green): eleven sticks were aligned in a straight line with 1 m-spacing and two sticks to the sides with 5 m distance to the main line. Four additional sticks (*validation sticks*, black) were distributed inside the area. b) Allocation of GCPs (ground control points) during the process of DEM (digital elevation model) generation. The top of the glass fibre sticks was used as GCP and manually checked for correct alignment (c).

Varying number of GCPs

DEMs for the validation area were generated following the same workflow in Agisoft PhotoScan as for the main study area. Previous (SfM) studies suggest the usage of several, but at least three, fixed locations as GCPs (e.g., James and Robson, 2012; Westoby et al., 2012; Fonstad et al., 2013; Smith et al., 2016; Cimoli et al., 2017). To assess the robustness of our SfM workflow regarding the number of used GCPs, we performed a sensitivity test using five, eight or 13 GCPs, and compared the DEM-derived snow heights at the validation sticks to manually measured reference snow heights. Mean differences, variances and RMSEs are averaged for all three dates (16.06., 27.06., and 09.07.2018, Table C2). Based on this analysis, we conclude that using more GCPs leads to an overall better representation. Further parameters as the image quality, the snow surface structures, the light conditions, and the cloud cover, especially for smooth snow surfaces, influence the quality of DEMs as well (Harder et al., 2016; Fernandes et al., 2018).

Camera-to-object distance and local snow height

The accuracy of DEM-derived snow heights depends on all steps involved in the photogrammetry SfM workflow. This includes the distance between the camera and the object, i.e., the snow surface in our case (Basnet et al., 2016). We therefore assessed the accuracy of DEM-derived snow height data at the validation sticks for different camera-to-object distances (between 3.8 m and 7 m) and found no dependency on the distance between camera and snow surface.

Table C2. Accuracy measures for varying numbers of GCPs used for the DEM generation. Mean differences, variances and RMSEs between DEM-derived and manually measured snow heights using five, eight or 13 GCPs are shown here. Values are averaged for all three dates on which DEMs are available for the validation area (i.e., 16.06., 27.06., and 09.07.2018).

Number GCPs	5	8	13
Mean difference (cm)	0.09	-0.21	-0.32
Variance (cm^2)	2.38	2.30	1.65
RMSE (cm)	1.48	1.46	1.27

Since the validation points are distributed on different local surface structures, we further analysed the accuracy of these varying snow heights. We also found no dependence regarding the relative snow height.

Inaccurate GCPs

450 Inaccuracies in the GCPs can be caused either by misaligned glass fibre sticks or by misplaced GCP locations during the processing. As this is the basis of the entire DEM generation, we evaluated both possible error sources by using the additional data from the validation area. Mean differences, variances, and RMSEs between DEM-derived and manually measured snow heights are calculated for the snow heights at the validation sticks.

The x-, y-, and z-coordinates of the 13 GCPs, used for the DEM generation, were manually changed to account for misaligned
455 sticks. Deviations from the documented coordinates were independently drawn from a normal distribution with a mean of 0 cm and a standard deviation of 2 cm, and were added to the initial input marker coordinates in Agisoft PhotoScan leading to the scenarios a) to e) below. Furthermore, manual misalignment of GCP locations in Agisoft PhotoScan was simulated by deliberately misplaced GCPs (scenario f).

    a) Change of x-coordinates (deviations along the main area).

460   b) Change of y-coordinates (deviations from the arbitrary chosen zero-line).

    c) Change of z-coordinates (deviations in the height of the stick top).

    d) Change of x- and y-coordinates by combining the deviations from a) and b).

    e) Change of x-, y- and z-coordinates by combining the deviations from a), b) and c).

    f) All 13 GCPs were manually set to the left and right margins of the sticks. The normal coordinates without changes were
465   used.

The DEM-derived snow heights from each of these cases is referenced to a DEM assuming perfectly aligned sticks and correct GCP input marker coordinates. Mean deviations between changed and initial DEMs range from -0.09 to 0.09 cm, variances from 0.02 to 0.97 cm^2, and RMSEs from 0.14 to 0.99 cm (Table C3). Based on this assessment, we conclude that

inaccurate distributions of GCPs (e.g., tilted sticks and inaccuracies in the x-, y- or z-coordinates, scenarios a to e) result in an

470 uncertainty of less than 1 cm. Changing the marker position (scenario f) has an even smaller effect on the overall accuracy of the final DEM (Table C3).

Table C3. Accuracy measures for inaccurate GCP coordinates and positions. Mean differences, variances, and RMSEs between normal DEM-derived snow heights and DEM-derived snow height with altered input marker coordinates or GCP positions. Scenarios a) to f) are explained in the text above.

Scenario	a)	b)	c)	d)	e)	f)
Mean difference (cm)	0.04	-0.09	-0.09	0.06	0.08	0.09
Variance (cm^2)	0.02	0.03	0.84	0.02	0.97	0.01
RMSE (cm)	0.13	0.2	0.92	0.15	0.99	0.14

Summary

The here performed tests provide accuracy estimates which are in an acceptable range for the purpose of the study. A more detailed investigation between snow surface conditions and uncertainties is beyond the scope of this study.

475 *Author contributions.* TL, TM, MH and HCSL designed the study. AMZ and HCSL carried it out. AMZ generated the digital elevation models and performed the analyses. AMZ prepared the manuscript with contributions from all co-authors.

Competing interests. The authors declare that they have no conflict of interest.

Acknowledgements. stitute, Helmholtz Centre for Polar and Marine Research), Japan (National Institute of Polar Research and Arctic Challenge for Sustainability), Norway (University of Bergen and Bergen Research Foundation), Switzerland (Swiss National Science Foundation),
480 France (French Polar Institute Paul-Emile Victor, Institute for Geosciences and Environmental research) and China (Chinese Academy of Sciences and Beijing Normal University). We further thank the AWI workshop for the construction of the photogrammetry equipment as well as Sonja Wahl, Anne-Katrine Faber, Melanie Behrens and Tobias Zolles for their help for the data acquisition during the 2018 field campaign. All numerical analyses were carried out by using the software R: A Language and Environment for Statistical Computing. TM acknowledges financing through the AWI Strategy Fund project *COMB-i*. This work has received funding from the European Research Council (ERC)
485 under the European Union's Horizon 2020 research and innovation program: Starting Grant-SNOWISO (grant agreement 759526).

References

Adams, M. S., Bühler, Y., and Fromm, R.: Multitemporal Accuracy and Precision Assessment of Unmanned Aerial System Photogrammetry for Slope-Scale Snow Depth Maps in Alpine Terrain, Pure and Applied Geophysics, 175, 3303–3324, https://doi.org/10.1007/s00024-017-1748-y, 2018.

490 Ahlstrøm, A. P., Gravesen, P., Andersen, S. B., van As, D., Citterio, M., Fausto, R. S., Nielsen, S., Jepsen, H. F., Kristensen, S. S., Christensen, E. L., Stenseng, L., Forsberg, R., Hanson, S., and Petersen, D.: A new programme for monitoring the mass loss of the Greenland ice sheet, Geological Survey of Denmark and Greenland (GEUS) Bulletin, 15, 61–64, 2008.

Albert, M. R. and Hawley, R. L.: Seasonal changes in snow surface roughness characteristics at Summit, Greenland: implications for snow and firn ventilation, Annals of Glaciology, 35, 2002.

495 Arthern, R. J., Winebrenner, D. P., and Vaughan, D. G.: Antarctic snow accumulation mapped using polarization of 4.3-cm wavelength microwave emission, Journal of Geophysical Research: Atmospheres, 111, https://doi.org/10.1029/2004JD005667, https://agupubs.onlinelibrary.wiley.com/doi/abs/10.1029/2004JD005667, 2006.

Baltsavias, E. P., Favey, E., Bauder, A., Bosch, H., and Pateraki, M.: Digital Surface Modelling by Airborne Laser Scanning and Digital Photogrammetry for Glacier Monitoring, The Photogrammetric Record, 17, 243–273, https://doi.org/10.1111/0031-868X.00182, https://onlinelibrary.wiley.com/doi/abs/10.1111/0031-868X.00182, 2001.

Basnet, K., Muste, M., Constantinescu, G., Ho, H.-C., and Xu, H.: Close range photogrammetry for dynamically tracking drifted snow deposition, Cold Regions Science and Technology, 121, 141–153, https://doi.org/10.1016/j.coldregions.2015.08.013, 2016.

Bühler, Y., Meier, L., and Ginzler, C.: Potential of Operational High Spatial Resolution Near-Infrared Remote Sensing Instruments for Snow Surface Type Mapping, IEEE Geoscience and Remote Sensing Letters, 12, 821–825, https://doi.org/10.1109/LGRS.2014.2363237, 2015.

505 Casado, M., Landais, A., Picard, G., Münch, T., Laepple, T., Stenni, B., Dreossi, G., Ekaykin, A., Arnaud, L., Genthon, C., Touzeau, A., Masson-Delmotte, V., and Jouzel, J.: Archival processes of the water stable isotope signal in East Antarctic ice cores, The Cryosphere, 12, 1745–1766, https://doi.org/10.5194/tc-12-1745-2018, https://www.the-cryosphere.net/12/1745/2018/, 2018.

Casado, M., Münch, T., and Laepple, T.: Climatic information archived in ice cores: impact of intermittency and diffusion on the recorded isotopic signal in Antarctica, Climate of the Past Discussions, 2019, 1–27, https://doi.org/10.5194/cp-2019-134, https://cp.copernicus.org/preprints/cp-2019-134/, 2019.

510 Cimoli, E., Marcer, M., Vandecrux, B., Bøggild, C. E., Williams, G., and Simonsen, S. B.: Application of Low-Cost UASs and Digital Photogrammetry for High-Resolutiong Snow Depth Mapping in the Arctic, Remote Sensing, 9, https://doi.org/doi:10.3390/rs9111144, 2017.

Dahl-Jensen, D., Kirk, M., Koldtoft, I., Popp, T., and Steffensen, J. P.: Field season 2019 East GReenland Ice core Project (EGRIP) 2015-2020: Third year of EGRIP deep drilling,, https://eastgrip.nbi.ku.documentation/2019/EGRIP2019FieldPlan_1stVersion.pdf, 2019.

515 Dansgaard, W.: Stable isotopes in precipitation, Tellus, 16, 436–468, https://doi.org/https://doi.org/10.3402/tellusa.v16i4.8993, 1964.

Deems, J. S., Painter, T. H., and Finnegan, D. C.: Lidar measurement of snow depth: a review, Journal of Glaciology, 59, 467–479, https://doi.org/10.3189/2013JoG12J154, 2013.

Dethloff, K., Schwager, M., Christensen, J. H., Kiilsholm, S., Rinke, A., Dorn, W., Jung-Rothenhäusler, F., Fischer, H., Kipfstuhl, S., and

520 Miller, H.: Recent Greenland Accumulation Estimated from Regional Climate Model Simulations and Ice Core Analysis, Journal of Climate, 15, 2821–2832, https://doi.org/10.1175/1520-0442(2002)015<2821:RGAEFR>2.0.CO;2, 2002.

ECMWF: ERA5 data documentation., https://software.ecmwf.int/wiki/display/CKB/ERA5+data+documentation, 2017.

Eisen, O., Frezzotti, M., Genthon, C., Isaksson, E., Magand, O., van den Broeke, M. R., Dixon, D. A., Ekaykin, A., Holmlund, P., Kameda, T., Karlöf, L., Kaspari, S., Lipenkov, V. Y., Oerter, H., Takahashi, S., and Vaughan, D. G.: Ground-based measurements of spatial and temporal variability of snow accumulation in East Antarctica, Reviews of Geophysics, 46, https://doi.org/10.1029/2006RG000218, https://agupubs.onlinelibrary.wiley.com/doi/abs/10.1029/2006RG000218, 2008.

Fernandes, R., Prevost, C., Canisius, F., Leblanc, S. G., Maloley, M., Oakes, S., Holman, K., and Knudby, A.: Monitoring snow depth change across a range of landscapes with ephemeral snowpacks using structure from motion applied to lightweight unmanned aerial vehicle videos, The Cryosphere, 12, 3535–3550, https://doi.org/10.5194/tc-12-3535-2018, https://tc.copernicus.org/articles/12/3535/2018/, 2018.

Fisher, D., Koerner, R. M., Paterson, W. S. B., Dansgaard, W., Gundestrup, N., and Reeh, N.: Effect of wind scouring on climatic records from ice-core oxygen-isotope profiles, Nature, 301, 205–209, https://doi.org/10.1038/301205a0, 1983.

Fisher, D., Reeh, N., and Clausen, H.: Stratigraphic Noise in Time Series Derived from Ice Cores, Annals of Glaciology, 7, 76–83, https://doi.org/10.3189/s0260305500005942, 1985.

Fonstad, M. A., Dietrich, J. T., Courville, B. C., Jensen, J. L., and Carbonneau, P. E.: Topographic structure from motion: a new developement in photogrammetric measurement, Earth Surface Processes and Landforms, 38, 421–430, https://doi.org/10.1002/esp.3366, 2013.

Gow, A. J.: On the Accumulation and Seasonal Stratification Of Snow at the South Pole, Journal of Glaciology, 5, 467–477, https://doi.org/10.3189/S002214300001844X, 1965.

Grohmann, C., Smith, M., and Riccomini, C.: Multiscale Analysis of Topographic Surface Roughness in the Midland Valley, Scotland, IEEE Transactions on Geoscience and Remote Sensing, 49, 1200–1213, 2011.

Groot Zwaaftink, C. D., Cagnati, A., Crepaz, A., Fierz, C., Macelloni, G., Valt, M., and Lehning, M.: Event-driven deposition of snow on the Antarctic Plateau: analyzing field measurements with SNOWPACK, The Cryosphere, 7, 333–347, https://doi.org/10.5194/tc-7-333-2013, https://www.the-cryosphere.net/7/333/2013/, 2013.

Harder, P., Schirmer, M., Pomeroy, J., and Helgason, W.: Accuracy of snow depth estimation in mountain and prairie environments by an unmanned aerial vehicle, The Cryosphere, 10, 2559–2571, https://doi.org/10.5194/tc-10-2559-2016, https://tc.copernicus.org/articles/10/2559/2016/, 2016.

Hawley, R. L. and Millstein, J. D.: Quantifying snow drift on Arctic structures: A case study at Summit, Greenland, using UAV-based structure-from-motion photogrammetry, Cold Regions Science and Technology, 157, 163 – 170, https://doi.org/https://doi.org/10.1016/j.coldregions.2018.10.007, http://www.sciencedirect.com/science/article/pii/S0165232X18301289, 2019.

James, M. R. and Robson, S.: Straightforward reconstruction of 3D surfaces and topography with a camera: Accuracy and geoscience application, Journal of Geophysial Research, 117, https://doi.org/doi:10/1029/2011JF002289, 2012.

James, M. R. and Robson, S.: Mitigating systematic error in topographic models derived from UAV and ground-based image networks, Earth Surface Processes and Landforms, 39, 1413–1420, https://doi.org/https://doi.org/10.1002/esp.3609, 2014.

Jouzel, J. and Merlivat, L.: Deuterium and oxygen 18 in precipitation: Modeling of the isotopic effects during snow formation, Journal of Geophysical Research: Atmospheres, 89, 11 749–11 757, https://doi.org/10.1029/JD089iD07p11749, https://agupubs.onlinelibrary.wiley.com/doi/abs/10.1029/JD089iD07p11749, 1984.

Karlsson, N. B., Razik, S., Hörhold, M., Winter, A., Steinhage, D., Binder, T., and Eisen, O.: Surface accumulation in Northern Central Greenland during the last 300 years, Annals of Glaciology, 61, 214–224, https://doi.org/10.1017/aog.2020.30, 2020.

Keutterling, A. and Thomas, A.: Monitoring glacier elevation and volume changes with digital photogrammetry and GIS at Gepatschferner glacier, Austria, International Journal of Remote Sensing, 27, 4371–4380, https://doi.org/10.1080/01431160600851819, 2006.

Kuhns, H., Davidson, C., Dibb, J., Stearns, C., Bergin, M., and Jaffrezo, J.-L.: Temporal and spatial variability of snow accumulation in central Greenland, Journal of Geophysical Research: Atmospheres, 102, 30 059–30 068, https://doi.org/10.1029/97JD02760, 1997.

Laepple, T., Hörhold, M., Münch, T., Freitag, J., Wegner, A., and Kipfstuhl, S.: Layering of surface snow and firn at Kohnen Station, Antarctica – noise or seasonal signal?, Journal of Geophysical Research: Earth Surface, p. 2016JF003919, https://doi.org/10.1002/2016JF003919, http://onlinelibrary.wiley.com/doi/10.1002/2016JF003919/abstract, 2016.

Li, L. and Pomeroy, J. W.: Probability of occurrence of blowing snow, Journal of Geophysical Research: Atmospheres, 102, 21 955–21 964, https://doi.org/10.1029/97JD01522, https://agupubs.onlinelibrary.wiley.com/doi/abs/10.1029/97JD01522, 1997a.

Li, L. and Pomeroy, J. W.: Estimates of threshold wind speeds for snow transport using meteorological data, Journal of Applied Meteorology, 36, 205–213, 1997b.

Madsen, M. V., Steen-Larsen, H. C., Hörhold, M., Box, J., Berben, S. M. P., Capron, E., Faber, A.-K., Hubbard, A., Jensen, M. F., Jones, T. R., Kipfstuhl, S., Koldtoft, I., Pillar, H. R., Vaughn, B. H., Vladimirova, D., and Dahl-Jensen, D.: Evidence of Isotopic Fractionation During Vapor Exchange Between the Atmosphere and the Snow Surface in Greenland, Journal of Geophysical Research: Atmospheres, 124, 2932–2945, https://doi.org/10.1029/2018JD029619, https://agupubs.onlinelibrary.wiley.com/doi/abs/10.1029/2018JD029619, 2019.

Masson-Delmotte, V., Steen-Larsen, H. C., Ortega, P., Swingedouw, D., Popp, T., Vinther, B. M., Oerter, H., Sveinbjornsdottir, A. E., Gudlaugsdottir, H., Box, J. E., Falourd, S., Fettweis, X., Gallée, H., Garnier, E., Gkinis, V., Jouzel, J., Landais, A., Minster, B., Paradis, N., Orsi, A., Risi, C., Werner, M., and White, J. W. C.: Recent changes in north-west Greenland climate documented by NEEM shallow ice core data and simulations, and implications for past-temperature reconstructions, The Cryosphere, 9, 1481–1504, https://doi.org/10.5194/tc-9-1481-2015, https://tc.copernicus.org/articles/9/1481/2015/, 2015.

Mosley-Thompson, E., Paskievitch, J. F., Gow, A. J., and Thompson, L. G.: Late 20th century increase in South Pole snow accumulation, Journal of Geophysical Research, 104, 3877–3886, https://doi.org/10.3189/172756502781831692, 1999.

Mosley-Thompson, E., McConnell, J. R., Bales, R. C., Li, Z., Lin, P.-N., Steffen, K., Thompson, L. G., Edwards, R., and Bathke, D.: Local to regional-scale variability of annual net accumulation on the Greenland ice sheet from PARCA cores, Journal of Geophysical Research: Atmospheres, 106, 33 839–33 851, https://doi.org/10.1029/2001JD900067, https://agupubs.onlinelibrary.wiley.com/doi/abs/10.1029/2001JD900067, 2001.

Münch, T., Kipfstuhl, S., Freitag, J., Meyer, H., and Laepple, T.: Regional climate signal vs. local noise: a two-dimensional view of water isotopes in Antarctic firn at Kohnen Station, Dronning Maud Land, Climate of the Past, 12, 1565–1581, https://doi.org/10.5194/cp-12-1565-2016, https://www.clim-past.net/12/1565/2016/, 2016.

Münch, T., Kipfstuhl, S., Freitag, J., Meyer, H., and Laepple, T.: Constraints on post-depositional isotope modifications in East Antarctic firn from analysing temporal changes of isotope profiles, The Cryosphere, 11, 2175–2188, https://doi.org/10.5194/tc-11-2175-2017, https://www.the-cryosphere.net/11/2175/2017/, 2017.

Naaim-Bouvet, F., Picard, G., Bellot, H., Arnaud, L., and Vionnet, V.: Snow Surface Roughness Monitoring Using Time-Lapse Terrestrial Laserscan, in: Proceedings, International Snow Science Workshop, Breckenridge, Colorado, pp. 649–654, 2016.

Nolan, M., Larsen, C., and Sturm, M.: Mapping snow depth from manned aircraft on landscape scales at centimeter resolution using structure-from-motion photogrammetry, The Cryosphere, 9, 1445–1463, https://doi.org/10.5194/tc-9-1445-2015, https://www.the-cryosphere.net/9/1445/2015/, 2015.

Persson, A., Langen, P. L., Ditlevsen, P., and Vinther, B. M.: The influence of precipitation weighting on interannual variability of stable water isotopes in Greenland, Journal of Geophysical Research: Atmospheres, 116, https://doi.org/10.1029/2010JD015517, https://agupubs.onlinelibrary.wiley.com/doi/abs/10.1029/2010JD015517, 2011.

Picard, G., Arnaud, L., Panel, J.-M., and Morin, S.: Design of a scanning laser meter for monitoring the spatio-temporal evolution of snow dpeth and its application in the Alps and in Antarctica, The Cryosphere, 10, 1495–1511, https://doi.org/doi:10.5194/tc-10-1495-2016, 2016.

Picard, G., Arnaud, L., Caneill, R., Lefebvre, E., and Lamare, M.: Observation of the process of snow accumulation on the Antarctic Plateau by time lapse laser scanning, The Cryosphere, 13, 1983 – 1999, https://doi.org/https://doi.org/10.5194/tc-13-1983-2019, 2019.

Rignot, E. and Thomas, R. H.: Mass Balance of Polar Ice Sheets, Science, 297, 1502–1506, https://doi.org/10.1126/science.1073888, https://science.sciencemag.org/content/297/5586/1502, 2002.

Ritter, F., Steen-Larsen, H. C., Werner, M., Masson-Delmotte, V., Orsi, A., Behrens, M., Birnbaum, G., Freitag, J., Risi, C., and Kipfstuhl, S.: Isotopic exchange on the diurnal scale between near-surface snow and lower atmospheric water vapor at Kohnen station, East Antarctica, The Cryosphere, 10, 1647–1663, https://doi.org/10.5194/tc-10-1647-2016, https://www.the-cryosphere.net/10/1647/2016/, 2016.

Schaller, C. F., Freitag, J., Kipfstuhl, S., Laepple, T., Steen-Larsen, H. C., and Eisen, O.: A representative density profile of the North Greenland snowpack, The Cryosphere, 10, 1991–2002, https://doi.org/10.5194/tc-10-1991-2016, http://www.the-cryosphere.net/10/1991/2016/, 2016.

Schlosser, E., Lipzig, N. v., and Oerter, H.: Temporal variability of accumulation at Neumayer station, Antarctica, from stake array measurements and a regional atmospheric model, Journal of Glaciology, 48, 87–94, https://doi.org/10.3189/172756502781831692, 2002.

Sime, L. C., Lang, N., Thomas, E. R., Benton, A. K., and Mulvaney, R.: On high-resolution sampling of short ice cores: Dating and temperature information recovery from Antarctic Peninsula virtual cores, Journal of Geophysical Research: Atmospheres, 116, https://doi.org/10.1029/2011JD015894, 2011.

Smith, M. W., Carrivick, J. L., and Quincey, D. J.: Structure from motion photogrammetry in physical geography, Progress in Physical Geography, 40, 247–275, https://doi.org/10.1177/0309133315615805, 2016.

Steen-Larsen, H. C.: Snow surface accumulation measured using Bamboo stake measurents, EastGRIP camp Greenland, May 2016, https://doi.org/10.1594/PANGAEA.921855, https://doi.pangaea.de/10.1594/PANGAEA.921855, 2020a.

Steen-Larsen, H. C.: Snow surface accumulation measured using SSA stake measurents, EastGRIP camp Greenland, May 2018, https://doi.org/10.1594/PANGAEA.921853, https://doi.pangaea.de/10.1594/PANGAEA.921853, 2020b.

Steen-Larsen, H. C., Masson-Delmotte, V., Hirabayashi, M., Winkler, R., Satow, K., Prié, F., Bayou, N., Brun, E., Cuffey, K. M., Dahl-Jensen, D., Dumont, M., Guillevic, M., Kipfstuhl, S., Landais, A., Popp, T., Risi, C., Steffen, K., Stenni, B., and Sveinbjörnsdóttir, A. E.: What controls the isotopic composition of Greenland surface snow?, Climate of the Past, 10, 377–392, https://doi.org/10.5194/cp-10-377-2014, https://www.clim-past.net/10/377/2014/, 2014.

Steffen, K. and Box, J.: Surface climatology of the Greenland Ice Sheet: Greenland Climate Network 1995–1999, Journal of Geophysical Research: Atmospheres, 106, 33 951–33 964, https://doi.org/10.1029/2001JD900161, https://agupubs.onlinelibrary.wiley.com/doi/abs/10.1029/2001JD900161, 2001.

Sturm, M., Liston, G. E., Benson, C. S., and Holmgren, J.: Characteristics and Growth of a Snowdrift in Arctic Alaska, U.S.A., Arctic, Antarctic, and Alpine Research, 33, 319–329, https://doi.org/10.1080/15230430.2001.12003436, https://doi.org/10.1080/15230430.2001.12003436, 2001.

Tonkin, T., Midgley, N., Cook, S., and Graham, D.: Ice-cored moraine degradation mapped and quantified using an unmanned aerial vehicle: A case study from a polythermal glacier in Svalbard, Geomorphology, 258, 1 – 10, https://doi.org/https://doi.org/10.1016/j.geomorph.2015.12.019, http://www.sciencedirect.com/science/article/pii/S0169555X15302397, 2016.

Vallelonga, P., Christianson, K., Alley, R. B., Anandakrishnan, S., Christian, J. E. M., Dahl-Jensen, D., Gkinis, V., Holme, C., Jacobel, R. W., Karlsson, N. B., Keisling, B. A., Kipfstuhl, S., Kjær, H. A., Kristensen, M. E. L., Muto, A., Peters, L. E., Popp, T., Riverman, K. L., Svensson, A. M., Tibuleac, C., Vinther, B. M., Weng, Y., and Winstrup, M.: Initial results from geophysical surveys and shallow coring of the Northeast Greenland Ice Stream (NEGIS), The Cryosphere, 8, 1275–1287, https://doi.org/10.5194/tc-8-1275-2014, https://www.the-cryosphere.net/8/1275/2014/, 2014.

van de Wal, R., Greuell, W., van den Broeke, M., Reijmer, C., and Oerlemans, J.: Surface mass-balance observations and automatic weather station data along a transect near Kangerlussuaq, West Greenland, Annals of Glaciology, 42, 311–316, https://doi.org/10.3189/172756405781812529, 2005.

van der Veen, C. J. and Bolzan, J. F.: Interannual variability in net accumulation on the Greenland Ice Sheet: Observations and implications for mass balance measurements, Journal of Geophysical Research: Atmospheres, 104, 2009–2014, https://doi.org/10.1029/1998JD200082, 1999.

van der Veen, C. J., Ahn, Y., Csatho, B. M., Mosley-Thompson, E., and Krabill, W. B.: Surface roughness over the northern half of the Greenland Ice Sheet from airborne laser altimetry, Journal of Geophysical Research: Earth Surface, 114, https://doi.org/10.1029/2008JF001067, 2009.

Veitinger, J., Sovilla, B., and Purves, R. S.: Influence of snow depth distribution on surface roughness in alpine terrain: a multi-scale approach, The Cryosphere, 8, 547–569, https://doi.org/10.5194/tc-8-547-2014, https://tc.copernicus.org/articles/8/547/2014/, 2014.

Weller, R., Traufetter, F., Fischer, H., Oerter, H., Piel, C., and Miller, H.: Postdepositional losses of methane sulfonate, nitrate, and chloride at the European Project for Ice Coring in Antarctica deep-drilling site in Dronning Maud Land, Antarctica, Journal of Geophysical Research: Atmospheres, 109, https://doi.org/10.1029/2003JD004189, 2004.

Westoby, M. J., Brasington, J., Glasser, N. F., Hambrey, M. J., and Reznolds, J. M.: 'Structure-from-Motion' photogrammetry: A low-cost, effective tool for geoscience applications, Geomorphology, 179, 300–314, https://doi.org/http://dx.doi.org/10.1016/j.geomorph.2012.08.021, 2012.

Zuhr, A., Münch, T., Steen-Larsen, H. C., Hörhold, M., and Laepple, T.: Snow height data generated with a Structure-from-Motion photogrammetry approach at the EGRIP camp site in 2018, https://doi.org/10.1594/PANGAEA.923418, https://doi.org/10.1594/PANGAEA.923418, 2020.